iScience

CellPress
OPEN ACCESS

Article

Regulation of purine metabolism connects KCTD13 to a metabolic disorder with autistic features

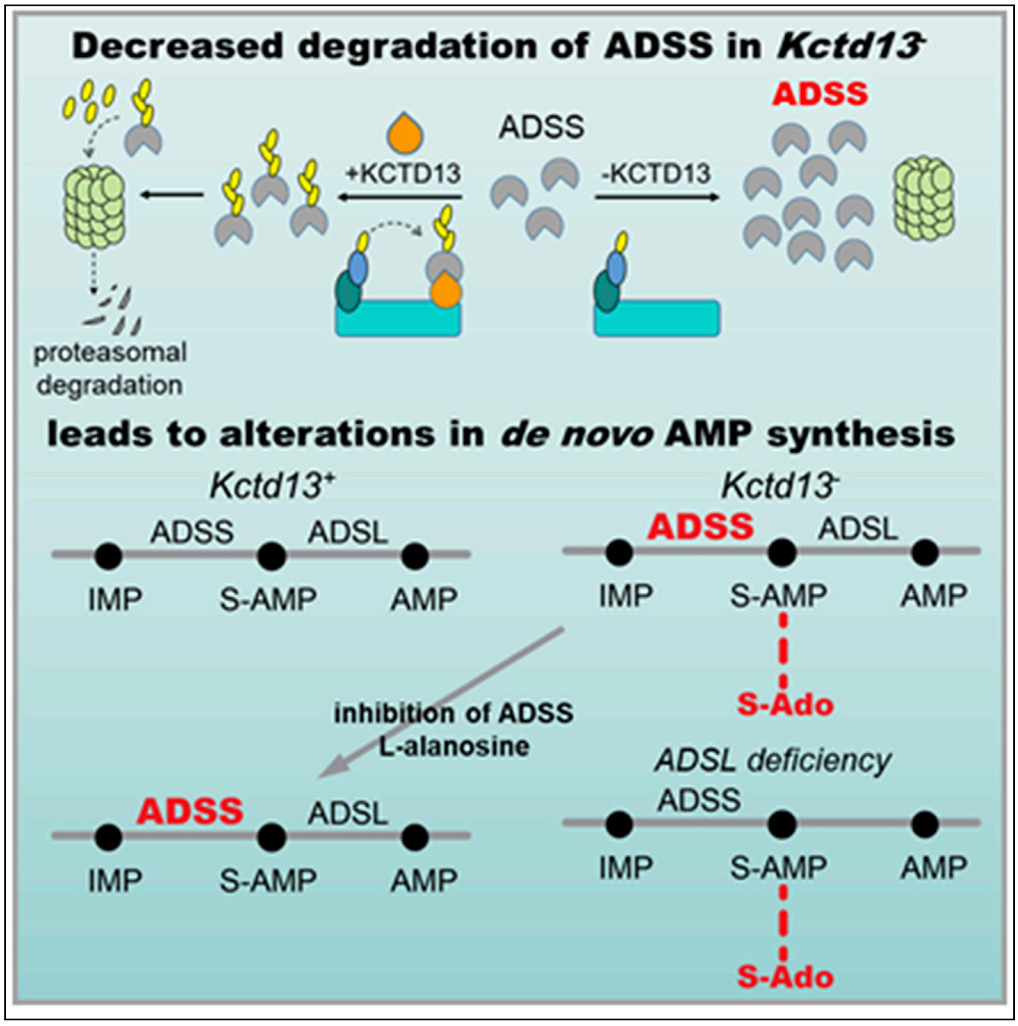

Jon M. Madison, Karen Duong, Ellen F. Vieux, ..., Morgan Sheng, Edward M. Scolnick, Jeffrey R. Cottrell

jmadison@broadinstitute.org

Highlights

KCTD13 deletion leads to decreases in ubiquitination and increases in levels of ADSS

KCTD13 deletion increases S-Ado levels, a metabolite observed in ADSL deficiency

Treatment of *KCTD13* deletion neurons with an ADSS inhibitor reduces S-Ado levels

Human *KCTD13* variants can alter ubiquitination of ADSS

Madison et al., iScience *24*, 101935
January 22, 2021
https://doi.org/10.1016/j.isci.2020.101935

iScience

CellPress
OPEN ACCESS

Article

Regulation of purine metabolism connects KCTD13 to a metabolic disorder with autistic features

Jon M. Madison,[1,11,*] Karen Duong,[1] Ellen F. Vieux,[1,7] Namrata D. Udeshi,[2] Sumaiya Iqbal,[1,5] Elise Requadt,[1] Shaunt Fereshetian,[2] Michael C. Lewis,[1,9] Antonio S. Gomes,[1,10] Kerry A. Pierce,[3] Randall J. Platt,[1,4,8] Feng Zhang,[1,4] Arthur J. Campbell,[1,5] Dennis Lal,[1,6] Florence F. Wagner,[1,5] Clary B. Clish,[3] Steven A. Carr,[2] Morgan Sheng,[1] Edward M. Scolnick,[1] and Jeffrey R. Cottrell[1]

Summary

Genetic variation of the 16p11.2 deletion locus containing the *KCTD13* gene and of *CUL3* is linked with autism. This genetic connection suggested that substrates of a CUL3-KCTD13 ubiquitin ligase may be involved in disease pathogenesis. Comparison of *Kctd13* mutant (*Kctd13*$^{-/-}$) and wild-type neuronal ubiquitylomes identified adenylosuccinate synthetase (ADSS), an enzyme that catalyzes the first step in adenosine monophosphate (AMP) synthesis, as a KCTD13 ligase substrate. In *Kctd13*$^{-/-}$ neurons, there were increased levels of succinyl-adenosine (S-Ado), a metabolite downstream of ADSS. Notably, S-Ado levels are elevated in adenylosuccinate lyase deficiency, a metabolic disorder with autism and epilepsy phenotypes. The increased S-Ado levels in *Kctd13*$^{-/-}$ neurons were decreased by treatment with an ADSS inhibitor. Lastly, functional analysis of human *KCTD13* variants suggests that *KCTD13* variation may alter ubiquitination of ADSS. These data suggest that succinyl-AMP metabolites accumulate in *Kctd13*$^{-/-}$ neurons, and this observation may have implications for our understanding of 16p11.2 deletion syndrome.

Introduction

Autism is a common neurodevelopmental disorder characterized by social interaction and communication deficits and repetitive behaviors (Hodges et al., 2020). Genetic association studies have identified a number of variants that contribute to risk for autism, including large hemizygous structural variants that either delete or duplicate sets of genes (Sanders et al., 2011; Takumi and Tamada, 2018). The association of these copy number variants with autism suggests that the dosage of genes in these intervals impacts risk for autism (Sanders et al., 2011, 2015). Among these copy number variants is the 16p11.2 deletion, which typically results in the loss of 27 genes (Sanders et al., 2011). It is unknown what gene or genes contribute to the phenotypes of the 16p11.2 deletion. To uncover the underlying causes of ASDs (autism spectrum disorders), an understanding of the potential contribution of these individual genes to autism risk is needed.

KCTD13 is one of the genes within the 16p11.2 deletion. Its protein product, KCTD13, is a BTB (BR-C, ttk, and bab) domain-containing protein that recruits substrates to ubiquitin ligase complexes for ubiquitination (Teng et al., 2019). Ubiquitination of proteins signals a number of functional consequences, such as targeting to the proteasome for degradation, altering complex assembly, and triggering protein endocytosis (Lydeard et al., 2013). Covalent modification of cellular proteins with ubiquitin is regulated by ubiquitin ligases, multi-protein complexes consisting of a scaffolding protein, which recruits a RING domain protein-E2 protein complex that brings ubiquitin to the ligase, and adapters, which recruit the substrate to the ligase. KCTD13 is an adapter that recruits cellular substrates to a CULLIN ubiquitin ligase complex. This KCTD13 ubiquitin ligase contains the scaffold protein CULLIN3 (CUL3), a RING domain protein, RBX1, and a ubiquitin-primed E2 protein (Chen et al., 2009). Exome sequencing studies have identified an excess of rare variants of *CUL3* in autism patients, suggesting a role in autism risk (O'Roak et al., 2012; Yuen et al., 2017; Stessman et al., 2017; Wang et al., 2016). Moreover, *CUL3* is in a locus associated with schizophrenia by GWAS (genome-wide association study) analysis, suggesting a potential role for CUL3 in schizophrenia,

[1]Stanley Center for Psychiatric Research, Broad Institute of MIT and Harvard, Cambridge, MA 02142, USA

[2]Proteomics Platform, Broad Institute of MIT and Harvard, Cambridge, MA 02142, USA

[3]Metabolomics Platform, Broad Institute of MIT and Harvard, Cambridge, MA 02142, USA

[4]McGovern Institute, Massachusetts Institute of Technology, Cambridge, MA 02142, USA

[5]Center for the Development of Therapeutics, Broad Institute of MIT and Harvard, Cambridge, MA 02142, USA

[6]Lerner Research Institute, Cleveland Clinic, 9500 Euclid Avenue, Cleveland, OH 44195, USA

[7]Present address: C4 Therapeutics, 490 Arsenal St, Watertown, MA 02472

[8]Present address: Department of Biosystems Science and Engineering, ETH Zurich, Mattenstrasse 26, 4058 Basel, Switzerland

[9]Present address: Sage Therapeutics, 215 First St, Cambridge, MA 02142

[10]Present address: Joslin Diabetes Center, One Joslin Place, Boston, MA 02215

[11]Lead contact

*Correspondence: jmadison@broadinstitute.org

https://doi.org/10.1016/j.isci.2020.101935

which shares some genetic overlap with autism (Schizophrenia Working Group of the Psychiatric Genomics, 2014). Taken together, these data suggest that a KCTD13-CUL3 ubiquitin ligase complex may play a role in autism pathogenesis, and identification of the substrates specified by KCTD13 might reveal relevant disease mechanisms. An understanding of these biochemical disease mechanisms may point to potential therapeutic interventions based on the restoration of these altered pathways.

Here, we used quantitative mass spectrometry-based proteomics to identify putative neuronal substrates of the KCTD13-CUL3 ubiquitin ligase. We identified adenylosuccinate synthetase (ADSS), a key regulator of the purine metabolism pathway, as a substrate of a KCTD13-ubiquitin ligase. Furthermore, we show that the metabolite succinyl-adenosine (S-Ado), a metabolite that is characteristic of adenylosuccinate lyase (ADSL) deficiency, an inborn error of metabolism with autism features, is elevated in *Kctd13*$^{-/-}$ neurons and that an inhibitor of ADSS corrects these elevated levels. Lastly, we show that human variation in the *KCTD13* gene results in alterations in ADSS ubiquitination levels in cellular assays. These data suggest that purine metabolism may be altered due to KCTD13 variation, and these results may have important implications for treating symptoms associated with 16p11.2 deletion syndrome.

Results

To identify neuronal substrates of KCTD13 ubiquitin ligase, a mouse with a 47-nucleotide deletion in exon 1 (*Kctd13*$^{-}$) was generated using CRISPR/Cas9 genome editing (Figure 1A). Western blots using a C-terminal KCTD13-specific antibody and lysates generated from the adult brain tissue (cortex, hippocampus, striatum) demonstrated absence of full-length KCTD13 protein in the brains of homozygous *Kctd13*$^{-/-}$ mice (cortex, hippocampus, and striatum, $n = 3$, $p < 0.0001$) (Figure 1B). In the cortex of heterozygous *Kctd13*$^{-/+}$ mice, we observed a significant 19% sd +/− 0.03 decrease ($n = 3$, $p < 0.01$, Student's t-test) in KCTD13 levels relative to wild type. Reduction of KCTD13 protein in the hippocampus and striatum of heterozygous *Kctd13*$^{-/+}$ mice did not reach statistical significance, suggesting there may be compensatory changes at the transcriptional or post-transcriptional level to regulate KCTD13 levels (hippocampus 7% sd +/− 0.02, $n = 3$, $p = 0.21$; striatum 18% sd +/− 0.17, $n = 3$, $p = 0.16$). Mice lacking full-length KCTD13 were viable and grossly normal.

Identification of ADSS as a substrate of a KCTD13 ubiquitin ligase

Due to the genetic linkage of the KCTD13-CUL3 complex to psychiatric disease, we hypothesized that alterations in the targets of this complex may play a role in disease pathogenesis following alteration in its expression or function. Typically, large copy number variants such as 16p11.2 are hemizygous in the genome but to improve or chances of identifying substrates of KCTD13 we utilized mass spectrometry-based proteomics to identify proteins with reduced ubiquitination in homozygous *Kctd13*$^{-/-}$ forebrain (striatum, hippocampus, and cortical) neurons. We used stable isotope labeling with amino acids in cell culture (SILAC) to metabolically label wild-type and *Kctd13*$^{-/-}$ dissociated forebrain neurons grown *in vitro* for 21 days with light and heavy amino acids, respectively. Cell lysates from the two label conditions were mixed and digested with trypsin, which removes the ubiquitin from proteins but leaves a Gly-Gly-ϵLys remnant moiety on the formerly ubiquitylated amino acid. These peptides were purified with an anti-Gly-Gly-ϵLys antibody (Udeshi et al., 2013) (Figure 1C). Both enriched Gly-Gly-ϵLys peptides, as well as peptides from samples prior to enrichment representing the global proteomes of *Kctd13*$^{-/-}$ and wild-type neurons, were measured in separate experiments by liquid chromatography-mass spectrometry (LC/MS) (Udeshi et al., 2013).

Mass spectrometric analysis of both sets of neurons grown in biological replicates identified 8,699 proteins (≥2 peptides/protein) (Table S1, Proteome) and 11,412 ubiquitinated sites from ~3,500 proteins (Table S3, All_Ubiquitin). Ubiquitinated sites were normalized by their corresponding protein changes in *Kctd13*$^{-/-}$ and wild-type neurons to account for protein stability changes (Figure 1E; Table S2 Ub_Proteome_norm). Protein substrates of the KCTD13-CUL3 ubiquitin ligase that are subject to degradation by the 26S proteasome were predicted to show (1) decreased levels of peptides containing Gly-Gly-ϵLys remnants and (2) increased total peptide levels in *Kctd13*$^{-/-}$ relative to wild-type neurons. Comparison of *Kctd13*$^{-/-}$ and wild-type neuron ubiquitylomes revealed levels of ubiquitination were decreased for 5 peptides from 4 separate proteins, while ubiquitination increased for 20 peptides from 19 proteins (modT test adjusted p value < 0.01) (Figure 1D; Table S2). Comparison of the total proteomes revealed 83 proteins whose levels were increased, while three proteins were significantly decreased in the *Kctd13*$^{-/-}$ neurons (modT test adjusted p-val < 0.01) (Figure 1E; Table S1). Comparison of regulated proteins identified in the

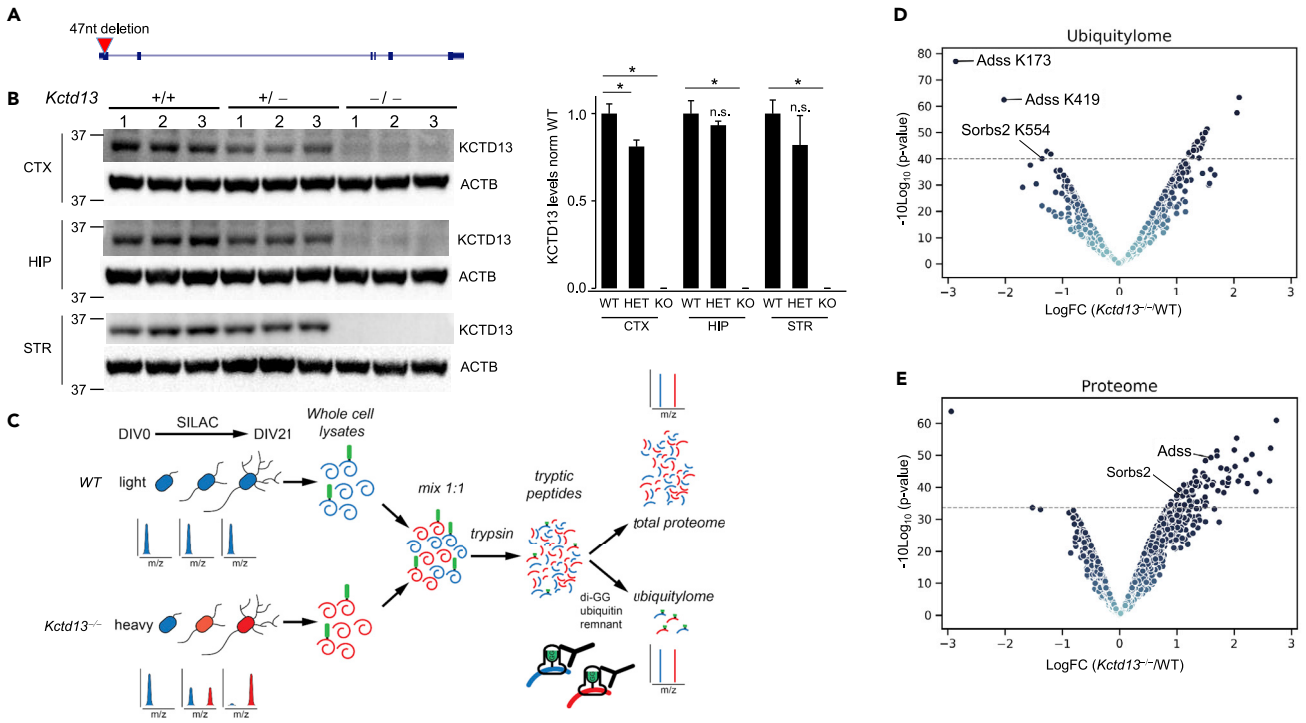

Figure 1. ADSS is a putative target of a KCTD13 ubiquitin ligase

(A) A *Kctd13* deletion mouse was created by targeting the first exon with CRIPSR/Cas9. A 47-nucleotide deletion was introduced in the first exon leading to a frameshift. Error bars indicate standard deviation of the mean.

(B) Western blots of whole-cell lysates from the cerebral cortex, hippocampus and striatum showed that in homozygous deletion mice, the KCTD13 protein was absent. In the cortex of heterozygous mice, the protein levels were significantly reduced (0.81 sd ± 0.3, t test p-val = 0.007).

(C) A schematic depicting the workflow for SILAC labeling of wild-type and *Kctd13*$^{-/-}$ neurons and subsequent quantitation of ubiquitin and total protein levels by global proteomics.

(D) Volcano plot of log2 fold-change of protein changes in *Kctd13*$^{-/-}$ vs. WT neurons (LogFC(*Kctd13*$^{-/-}$/WT)). The dotted line indicates an adjusted p value = 0.05 followed by a one-sample moderated t-test. The two significantly decreased sites of ADSS ubiquitination are indicated. The gradient hue (white [p-val = 0.99] to dark blue [p-val = 0.0035]) of the volcano plot reflects the adjusted p values resulting from the moderated t test.

(E) Volcano plot of ubiquitination sites normalized by corresponding protein level changes in *Kctd13*$^{-/-}$ vs. WT neurons (LogFC(*Kctd13*$^{-/-}$/WT)). The dot corresponding to ADSS is indicated in the figure. The dotted line indicates an adjusted p value = 0.05 followed by a one-sample moderated t-test. The gradient hue (white [p-val = 0.99] to dark blue [p-val = 0.00019]) of the volcano plot reflects the adjusted p values resulting from the moderated t test. CTX, cortex; HIP, hippocampus; STR, striatum.

ubiquitylome and total proteome revealed two proteins with both decreased ubiquitination and increased total protein level in *Kctd13*$^{-/-}$ neurons, ADSS (ubiquitination, K173 LogFC −2.8 and K419 LogFC −2.01, adjusted p value < 0.01; proteome, LogFC 1.6, adjusted p value < 0.01, modT test adjusted), and Sorbin and SH3 domain-containing protein 2 (SORBS2) (ubiquitination, K554, LogFC −1.4, adjusted p value < 0.01; proteome, LogFC 1.1, adjusted p value < 0.01, modT test adjusted). While we focused on ADSS due to the identification of multiple decreased ubiquitinated peptides, the magnitude of the change in these ubiquitinated peptides and the increased abundance of ADSS peptide levels, SORBS2 and the other 78 proteins whose abundance goes up in the *Kctd13*$^{-/-}$ neurons could also represent substrates of the KCTD13 ubiquitin ligase. This set of proteins was enriched (DAVID, FDR <0.05) for virus response proteins (7/79 genes, adjusted p-val 5.8x10^{-4}) and extracellular matrix proteins (11/79, adjusted p-val 5.0x10^{-6}).

To verify that ADSS levels are increased in *Kctd13*$^{-/-}$ neurons, dissociated neurons from wild-type and *Kctd13*$^{-/-}$ E18 mouse embryos were grown for 21 days *in vitro*. Western blots performed on *Kctd13*$^{-/-}$ neuron cultures confirmed that levels of ADSS are increased ~2.3-fold (WT avg. = 0.68 sd +/− 0.25, *Kctd13*$^{-/-}$ avg. = 1.58 sd +/− 0.40) (n = 3, p < 0.01) in *Kctd13*$^{-/-}$ lysates compared to wild type (Figure 2A). These data suggest that ADSS is a substrate of a KCTD13 ubiquitin ligase and that ubiquitylated ADSS is subsequently degraded by the 26S proteasome. These data are consistent with previous work, which identified ADSS in complexes containing CUL3, KCTD13; ADSS was the only overlapping protein in these data (Bennett et al., 2010).

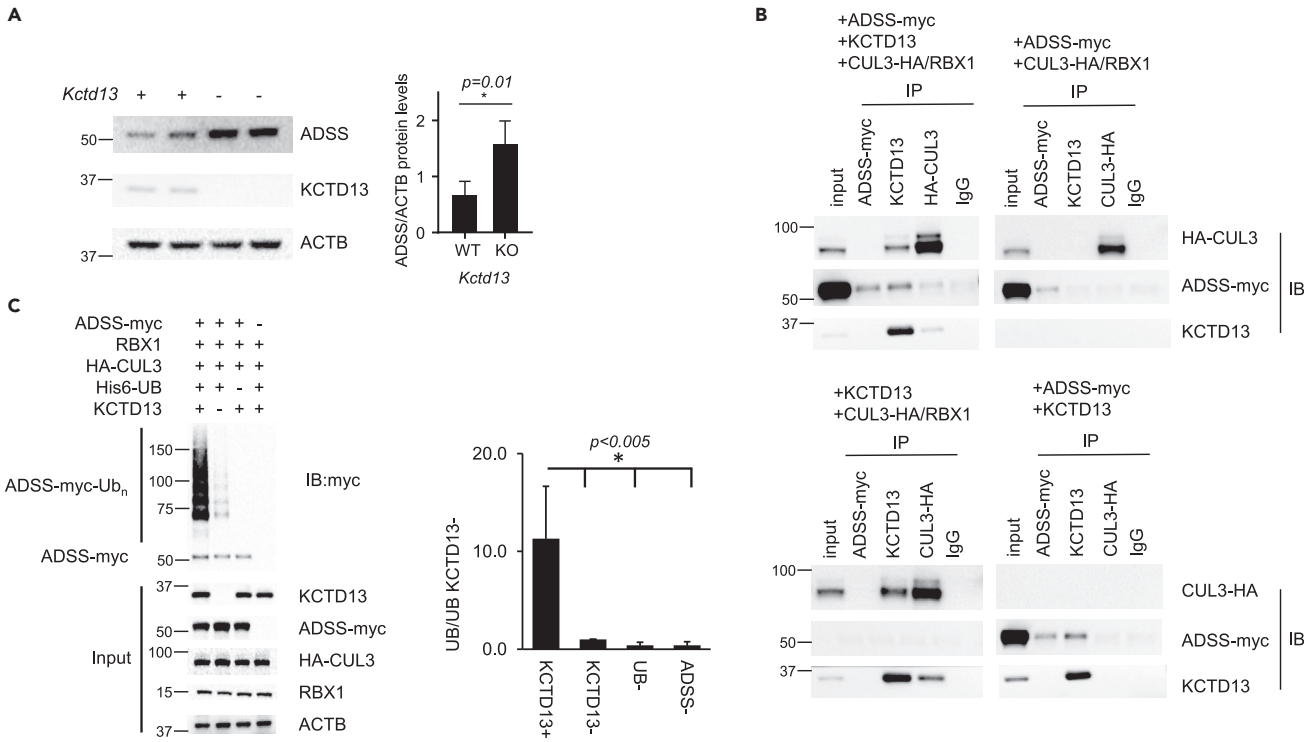

Figure 2. ADSS is associated with and ubiquitinated by a CUL3-KCTD13 complex

(A) Western blots show that levels of neuronal ADSS were increased in *Kctd13*$^{-/-}$ mice relative to wild-type mice in dissociated neurons grown *in vitro* for 21 days. * indicates significance, t test p = 0.01. Error bars indicate standard deviation of the mean.

(B) ADSS-CUL3-KCTD13 proteins were immunoprecipitated together. ADSS-myc, HA-CUL3, and KCTD13 were transfected into HEK cells. Immunoprecipitates were collected using antibodies specific for the MYC epitope for ADSS-myc, KCTD13, and for the HA epitope for CUL3-HA. IgG immunoprecipitates were run as a negative control. Western blots were run and probed with the indicated antibodies. Additional immunoprecipitations were carried out in which one of the components was left out as indicated in the figure.

(C) ADSS ubiquitination was KCTD13 dependent in a His-ubiquitin assay. *ADSS-myc*, *KCTD13*, *HA-CUL3*, and *6xhistidine-ubiquitin* plasmids were transfected into HEK cells in the combinations indicated. His-ubiquitin conjugated proteins were collected and Western blots with myc antibody were performed to identify His-ubiquitinated ADSS. Total whole-cell lysates were probed on Western blots with the indicated antibodies to verify the expression of the indicated proteins. * indicates significance, t test p < 0.005. Error bars indicate standard deviation of the mean.

Cullin ubiquitin ligases are multi-subunit complexes consisting of a scaffolding protein and an adapter protein that recruits substrates to be ubiquitinated (Zheng and Shabek, 2017), a model predicting that CUL3, KCTD13, and ADSS form a complex. To test this hypothesis, we performed co-immunoprecipitations (co-IP) from 293T HEK cell lysates expressing the individual components of the KCTD13-CUL3 ubiquitin ligase complex: KCTD13, CUL3 tagged with the hemagglutinin epitope (HA) (CUL3-HA), RBX1, the RING BOX protein that co-assembles with CUL3, and ADSS tagged with the myc epitope (ADSS-myc) (Figure 2B). Indeed, when KCTD13-specific antibodies were used to immunoprecipitate (IP) KCTD13 complexes, both ADSS-myc and HA-CUL3 were identified. When HA antibodies were used to IP HA-CUL3, KCTD13 was readily identified, while ADSS was close to background levels. Lastly, when antibodies against myc were used to IP ADSS, neither KCTD13 nor CUL3 was visible, suggesting only a subset of the total ADSS is associated with the CUL3-KCTD13 complex or association of the myc antibody with ADSS-myc disrupts the complex. When we omitted KCTD13 from the transfections, we did not IP ADSS or CUL3, but when we omitted CUL3 from the transfections, KCTD13 immunoprecipitated ADSS (Figure 2B). Taken together, these data suggest a complex of ADSS, KCTD13, and CUL3 can form in cells, consistent with KCTD13 acting as a substrate adapter to recruit ADSS to CUL3.

Our data suggest that KCTD13 may regulate the ubiquitination of ADSS in cells. To determine whether ADSS can be ubiquitinated in a KCTD13-dependent manner, we performed cell ubiquitination assays. Plasmids for expressing *KCTD13*, *ADSS-myc*, *HA-CUL3*, *RBX1*, and 6X histidine-tagged ubiquitin (His-Ub) were transfected into 293T HEK cells. After two days, cells were treated with bortezomib to inhibit the

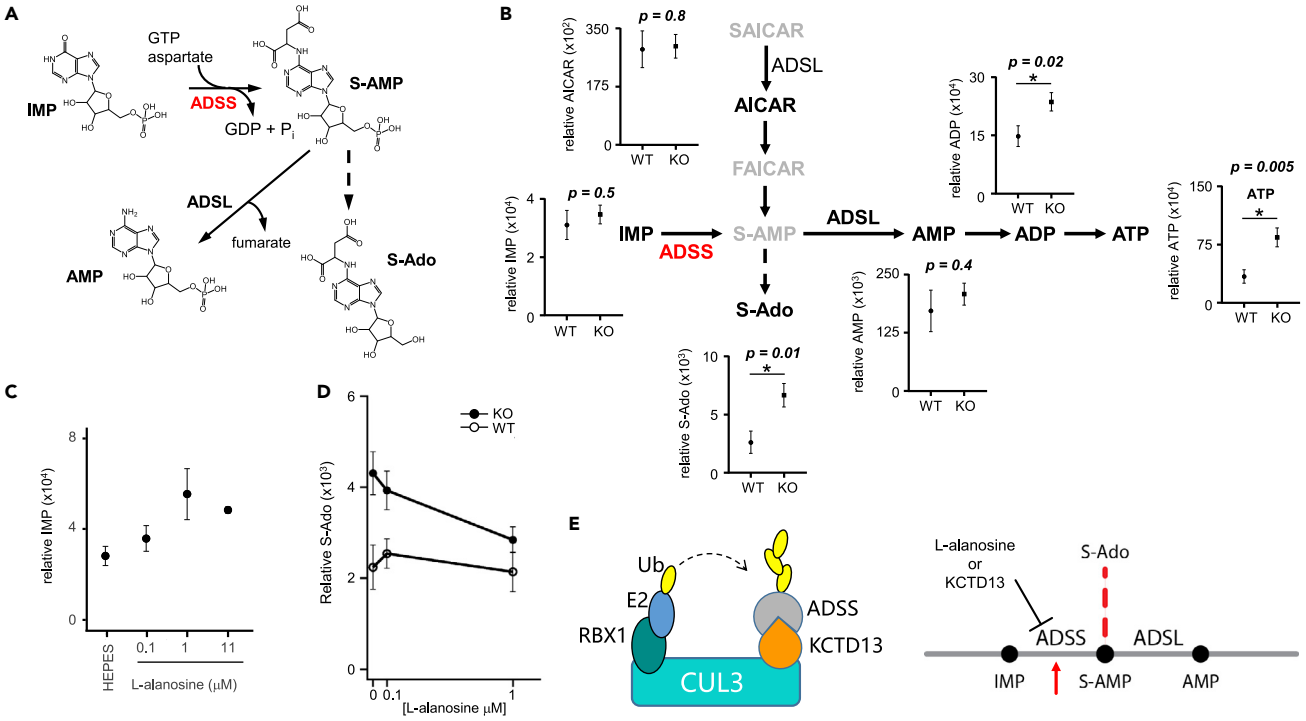

Figure 3. Succinyl-adenosine (S-Ado) is increased in *Kctd13*$^{-/-}$ neurons

(A) A schematic of AMP biosynthesis is shown.

(B) Purine metabolites were increased in *Kctd13*$^{-/-}$ neurons. Core purine metabolism is shown with relative levels of each metabolite summarized. S-Ado, ADP, ATP, and AMP were significantly altered. * indicates significance, t test, $p < 0.05$. Error bars indicate standard deviation of the mean.

(C) Titration of L-alanosine in HEPES in increasing concentration into mouse neuronal cultures resulted in increased relative levels of IMP. Error bars indicate standard deviation of the mean.

(D) S-Ado levels were reduced to wild-type levels by L-alanosine in *Kctd13*$^{-/-}$ neurons. Data from 3 experiments were summarized for wild-type and *Kctd13*$^{-/-}$ neurons treated with L-alanosine. The two-way ANOVA found the interaction to be significant ($F(2,66) = 3.192$, $p = 0.05$). Error bars indicate standard deviation of the mean.

(E) Model for KCTD13 regulation of ADSS and purine metabolism. (Left panel) KCTD13 recruits ADSS to a CULLIN3 ubiquitin ligase where it is ubiquitylated. (Right panel) KCTD13 functionally acts as a negative regulator of ADSS levels. Deletion of KCTD13 resulted in elevated ADSS levels (red arrow). Elevated ADSS levels resulted in increased S-Ado levels which were decreased by the ADSS inhibitor L-alanosine.

proteasome, and protein lysates were collected under denaturing conditions. His-Ub-protein conjugates were then isolated with Ni-NTA beads and blotted for the presence of the substrate ADSS-myc. As shown in Figure 2C, co-expression of all components led to a significant, ~11-fold increase in ubiquitination of ADSS-myc (Ub-ADSS). Omission of *KCTD13* from transfections reduced the Ub-ADSS conjugates to background levels. Furthermore, omission of His-Ub or ADSS also led to the elimination of the Ub-ADSS signal (values normalized to Kctd13^{-}; WT = 11.3 sd +/− 5.4, Kctd13^{-} = 1, ADSS^{-} = 0.4 sd +/− 0.3, Ub^{-} = 0.4 sd +/− 0.4; n = 3, $p < 0.005$; Student's t-test). In total, our data are consistent with the presence of a KCTD13-containing ubiquitin ligase complex that regulates ADSS levels.

S-Ado levels are regulated by KCTD13

The proteomic data suggest that a KCTD13-dependent ubiquitin ligase negatively regulates the levels of ADSS in cells. ADSS catalyzes the first committed step in the *de novo* synthesis of purines by converting inosine monophosphate (IMP) into adenylosuccinate (S-AMP) (Stayton et al., 1983). The enzyme ADSL subsequently converts adenylosuccinate to adenosine monophosphate (AMP) (Figure 3A), and AMP is subsequently phosphorylated to ADP and ATP. ADSL also plays an upstream role in IMP generation, catalyzing the conversion of succinylaminoimidazole carboxamide ribotide (SAICAR) to aminoimidazole carboxamide ribotide (AICAR). Notably, homozygous loss of function of the *ADSL* gene causes ADSL deficiency, a metabolic disorder associated with developmental delay, motor dysfunction, and autistic features. A key feature of ADSL deficiency is the accumulation of SAICAR and of a metabolite of unknown activity called succinyl-

adenosine (S-Ado) in the cerebrospinal fluid (CSF) and plasma of affected individuals, whereas normal individuals have little or none of S-Ado in their CSF or plasma (Baresova et al., 2012; Jurecka et al., 2015). It was previously demonstrated that purine pathway deficits could be observed in ADSL deficiency patient fibroblasts grown *in vitro* (Baresova et al., 2012; Jurecka et al., 2015). Similarly, changes in S-AMP and upstream metabolites were correlated with changes in ADSS levels or activity in a human pancreatic beta cell line (Gooding et al., 2015). These experiments suggested that alterations in KCTD13 regulation of ADSS might lead to cellular changes in purine metabolism and led us to explore purine biosynthesis in *Kctd13*$^{-/-}$ neurons.

To test if there were alterations in purine metabolites following KCTD13 deletion in neurons, we examined changes in cellular metabolites in mouse *Kctd13*$^{-/-}$ neurons *in vitro*. We cultured *Kctd13*$^{-/-}$ and wild-type forebrain neurons for 21 days and measured polar metabolites in cell extracts using liquid chromatography-tandem mass spectrometry (Figure 3B). Of the purine metabolites downstream of ADSS, we found significantly increased levels of ATP (KO = $84.1x10^{-4}$ sd +/− $12.2x10^{-4}$, WT = $33.7x10^{-4}$ sd +/− $8.7x10^{-4}$, fold = 1.7; p = 0.05, Student's t-test), ADP (, KO = $23.6x10^{-4}$ sd +/− $2.3x10^{-4}$, WT = $14.7x10^{-4}$ sd +/− $2.6x10^{-4}$, fold = 1.4; p < 0.01, Student's t-test), and S-Ado (KO = $6.6x10^{-4}$ sd +/− $0.9x10^{-4}$, WT = $2.6x10^{-4}$ sd +/− $1.0x10^{-4}$, fold = 2.5; p < 0.01, Student's t-test). AMP levels also increased, but the change did not reach statistical significance (KO = $20.7x10^{-4}$ sd +/− 2.3, WT = $17.2x10^{-4}$ sd +/− $4.4x10^{-4}$, fold = 1.4; p = 0.07, Student's t-test). Upstream of ADSS, we found that IMP (KO = $3.5x10^{-4}$ sd +/− $0.3x10^{-4}$, WT = $3.1x10^{-4}$ sd +/− $0.5x10^{-4}$, fold = 1.1; p = 0.5, Student's t-test) levels were unchanged, and similarly, in the branch upstream of S-AMP, AICAR levels (KO = $2.9x10^{-4}$ sd +/− 0.4, WT = 2.8x10-4 sd +/−0.5, fold 1.1; p = 0.5, Student's t-test) were unchanged, while S-AMP and SAICAR were not observed. These data suggest that an increase in ADSS protein levels leads to elevated ADSS activity and higher steady-state levels of ADSS-derived metabolites. Among these metabolites, S-Ado, one of the key metabolites observed in ADSL deficiency, showed the biggest increase in the *Kctd13*$^{-/-}$neurons, highlighting a biochemical phenotype that is shared between ADSL deficiency and *Kctd13* deletion.

The increase in purine metabolites found in the *Kctd13*$^{-/-}$ mouse cultured neurons and previously associated with ADSL deficiency suggested inhibition of the ADSS enzyme could reverse the observed alterations in purine levels. To confirm that these S-Ado changes were due to enhanced ADSS activity and to determine if we could normalize changes in these purine metabolites with a small molecule inhibitor of ADSS, we treated neuronal cultures with L-alanosine, a specific inhibitor of ADSS (Tyagi and Cooney, 1980). To determine suitable concentrations of L-alanosine to use on primary dissociated neurons, we titrated L-alanosine into neuronal growth media; wild-type neurons grew normally in L-alanosine concentrations less than 11.3 μM (data not shown). Consistent with inhibition of ADSS in these titrations, treatment of wild-type mouse forebrain neurons for 12 hr with L-alanosine, as compared to the vehicle HEPES (2-[4-(2-hydroxyethyl)piperazin-1-yl]ethanesulfonic acid), led to an increase in the levels of the upstream metabolite IMP (Figure 3C). To measure the effects of L-alanosine in *Kctd13*$^{-/-}$ neurons, forebrain neurons from wild-type and *Kctd13*$^{-/-}$ mice were grown *in vitro* for 20 days. On day 20, neurons were treated with L-alanosine at 1.1 μM and 0.1 μM for 12 hr, and then, cellular metabolites were collected and measured by LC/MS (Figure 3C). Under these conditions, S-Ado levels were reduced in a concentration-dependent manner from an average of 4305 sd +/− 474 (vs wt, 2241 sd +/− 487) in 0 μM L-alanosine to 2842 sd +/− 283 (vs wt, 2139 sd +/− 439) in 1.1 μM L-alanosine (Figure 3D). ANOVA (analysis of variance) revealed that the two-way interaction was significant ($F(2,66) = 3.192$, p = 0.05), and there was a significant reduction of S-Ado levels following L-alanosine treatment in *Kctd13*$^{-/-}$ neurons. In contrast to S-Ado levels in *Kctd13*$^{-/-}$ neurons, S-Ado was not significantly decreased in wild-type neurons; these wild-type S-Ado levels could be background levels due to our culture conditions. These data suggest that the increase in S-Ado levels in the *Kctd13*$^{-/-}$ neurons are due to changes in ADSS activity and that inhibition of ADSS could reduce S-Ado levels in KCTD13-deficient neurons (Figure 3E).

KCTD13 variants that disrupt ubiquitination of ADSS

To gain additional evidence that KCTD13 is involved in ADSS ubiquitination, we performed functional studies on a set of KCTD13 coding mutations and variants of unknown function and tested them for effects on ADSS ubiquitination. These variants were selected from the gnomAD database which contains variants from many disease-specific and population genetic exome sequencing studies (https://gnomad.broadinstitute.org/). Among the variants we selected were variants from healthy individuals and variants from patients with schizophrenia (although these variants are not necessarily causal or disease linked)

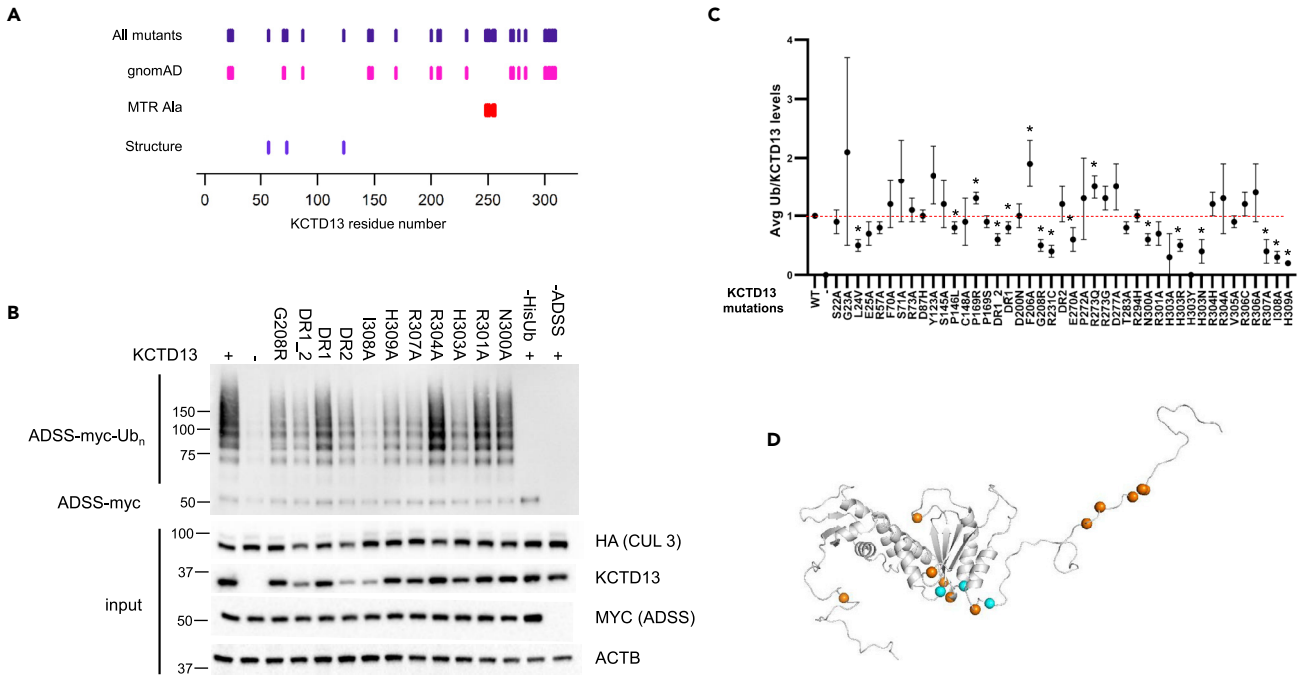

Figure 4. Specific KCTD13 mutations reduce ADSS ubiquitination

(A) A raster diagram indicates the KCTD13 variant positions that were analyzed. The top row (indigo tick marks) indicates all residue positions that were mutated. The second (magenta tick marks) row shows gnomAD variants. The third row (red tick marks) indicates a set of residues identified by the MTR viewer. The fourth row (purple tick marks) indicates a set of residues nominated by structural analysis.

(B) A representative Western blot is shown of His6-Ubiquitin assays of KCTD13-dependent ubiquitination of ADSS for different KCTD13 mutations and wild-type KTD13. Western blots of total protein lysates indicate the levels of input proteins for each assay.

(C) Summary data of each KCTD13 mutation for n = 3 independent assays. * indicates significance compared to wild type, t test $p < 0.05$. Ubiquitination levels for each independent assay were normalized to KCTD13 levels. Data for each mutant are normalized to the level of wild-type KCTD13 ubiquitination of ADSS-myc.

(D) Loss-of-function mutations (orange balls) and gain-of-function mutations (cyan balls) that were identified as significantly different from wild type (Student's t-test $p < 0.05$) are indicated on a KCTD13 homology model.

(Figure 4A, gnomAD) (Karczewski et al., 2020). In addition, we mutated two regions identified by the Missense Tolerance Ratio (DR_1, DR_2), which identifies amino acid residues under purifying selection (ExAC v 2.0, gnomAD) (Figure 4A, MTR Ala) (Traynelis et al., 2017). Lastly, we also included three mutations based on their position in other KCTD-CUL3 crystal structures that were predicted to disrupt the KCTD-CUL3 interaction and potentially reduce ADSS ubiquitination (Figure 4A, STRUCTURE) (personal communication G. Prive). In total, 43 variants were introduced into *KCTD13* using site-directed mutagenesis, and in-cell ADSS ubiquitination assays were performed and levels of ADSS ubiquitination were measured by Western blot. As shown in Figures 4B and 4C, these variants were able to support different levels of ADSS ubiquitination (representative assays for all variants are shown in Figure S2). Twelve variants (27%) led to significantly decreased ADSS ubiquitination compared to wild type (ADSS ubiquitination normalized to levels of KCTD13; t test, $p < 0.05$) (amino acid changes: L24V, P146L, G208R, R231C, DR1(248–251), DR1_DR2, E270A, H303R, H303N, R307A, R308A, R309A) while three variants (5%) (amino acid changes: F206A, F273Q, P169R) led to significantly increased ubiquitination (Figure 4C). There was no correlation with disease (schizophrenia) or lack of disease. These results indicated specific KCTD13 residues may contribute to ADSS ubiquitination and suggested KCTD13 variants could have an impact on cell physiology.

Discussion

Here, we described the identification of substrates of KCTD13, a ubiquitin ligase substrate adapter found in the autism-associated 16p11.2 deletion region. We demonstrated that a KCTD13 containing ubiquitin ligase complex is a negative regulator of ADSS, a critical enzyme in the purine biosynthetic pathway. The loss of KCTD13 results in an increase in ADSS protein levels and elevation of the levels of purine

metabolites downstream of the ADSS catalyzed conversion of IMP to S-AMP. The most significantly elevated metabolite is S-Ado, a dephosphorylated form of S-AMP. These results suggest KCTD13 regulates purine metabolism through ADSS and when KCTD13 function is reduced in mouse neurons, similar to ADSL deficiency, an inborn error of de novo purine metabolism, S-Ado levels and other purine metabolites are elevated. ADSL deficiency has overlapping features with 16p11.2 deletion syndrome, such as seizures and autistic features. These results have important implications for understanding how biochemical and metabolic pathways might increase an individual's risk for autism or epilepsy phenotypes and may provide insight into how to treat symptoms associated with these disorders.

Identification of a KCTD13 ubiquitin ligase substrate

Identification of substrates of specific ubiquitin ligase adapters is important for our understanding of the biochemical details of cellular protein homeostasis such as what adapter sequences help specify certain substrates. In the case of KCTD13, identification of substrates of this adapter might also help clarify its role in 16p11.2 schizophrenia and autism disease associations. Our experiments (Figures 1C, 1D, 1E, and 2), consisting of ubiquitylome profiling, co-IP and His-Ub assays suggest ADSS is a bona fide substrate of a KCTD13 ubiquitin ligase. While both our co-IP and His-Ub experiments extend our results from mouse to human proteins, further co-IP and His-Ub experiments from mouse neurons may help further establish ADSS as a KCTD13 ubiquitin ligase substrate in neurons.

Purine metabolism in autism

Besides accumulation of ADSS protein, purine metabolism is dysregulated in neurons from KCTD13-deficient mice. The overproduction of S-Ado in the *Kctd13* knockout mouse neurons, which is similar to ADSL deficiency, led us to speculate that this change may influence the risk for autistic-like phenotypes. While our data suggest a biochemical connection between KCTD13 and ADSL deficiency through de novo purine synthesis and increased S-Ado levels, the role S-Ado plays in autism phenotypes is still unknown (Jurecka et al., 2015). Furthermore, while S-Ado shows the biggest change in our study, it is possible that other metabolites such as SAICAR, S-AMP (Gooding et al., 2015), or combinations of metabolites could cause the phenotypes observed. It has been suggested that SAICAR may be the metabolite responsible for ADSL deficiency phenotypes and that the S-Ado:SAICAR ratio is correlated with the severity of ADSL deficiency phenotypes. Yet, the correlation between SAICAR or the S-Ado:SAICAR ratio and the heterogeneous ADSL phenotypic presentation is not always clear, suggesting the involvement of these metabolites may be complicated and their actions may be modified by other physiological factors (Gitiaux et al., 2009; Zikanova et al., 2010). In our metabolomic assays, we were readily able to observe S-Ado but not SAICAR or S-AMP, making it unclear if SAICAR or S-AMP are altered in *Kctd13*$^{-/-}$ neurons or if they are rapidly metabolized to maintain normal levels. In addition, we observed altered levels of downstream purines such as AMP, ADP, and ATP. In addition to understanding which of these purine metabolites might be responsible for the phenotypes observed in ADSL deficiency and potentially 16p11.2 deletion syndrome, understanding the functional effects increased levels of S-Ado, SAICAR, S-AMP, or other purine metabolites have on brain development and function and the correlation with the severity of phenotype will be a key area for further investigation.

Other studies have reported brain and synaptic deficits associated with the 16p11.2 deletion. Portman et al. described deficits in basal ganglia circuits and behaviors in the 16p11.2 deletion mouse model (Portmann et al., 2014). In addition, recent data from in IPSC-derived human neurons and in a *Kctd13* deletion mouse suggest that the 16p11.2 and the *Kctd13* deletion influence synapse development and function (Deshpande et al., 2017; Escamilla et al., 2017). Escamilla et al. further suggest the physiological effects of *Kctd13* deletion are mediated by RHOA (Escamilla et al., 2017), and a previous gene expression bioinformatics study also implicated the KCTD13-CUL3-RHOA interaction in psychiatric disease (Lin et al., 2015). In our ubiquitination proteomics analysis, we did not observe a significant change in RHOA ubiquitination or RHOA steady-state levels in *Kctd13*$^{-/-}$ mice (Table S4). Overall, our findings suggest that, depending on the critical period of KCTD13 function in development or neuron function and the levels of S-Ado, inhibitors of ADSS might correct the KCTD13-dependent behavioral and functional deficits observed in these 16p11.2 model systems.

Therapeutic potential of ADSS inhibitors

Our data suggest a therapeutic hypothesis: inhibit ADSS activity to reduce symptoms associated with 16p11.2 syndrome. An inhibitor of ADSS, L-alanosine, can reduce the levels of S-Ado in our *Kctd13* deletion

neuronal cultures, which supports the notion that the elevated levels of S-Ado were due to higher levels of ADSS in *Kctd13*-deficient neurons. The potential for measuring S-Ado levels in patient samples such as CSF, plasma, or urine raises the possibility of using this metabolite as a diagnostic and pharmacodynamic biomarker. The next step toward evaluating this therapeutic hypothesis would be to demonstrate elevated S-Ado levels in both *Kctd13* deletion and 16p11.2 deletion animal models.

Taken together, our data suggest an intriguing and potential step toward an understanding of the molecular and cellular pathogenesis of an autism spectrum disorder. The genetic connection of two seemingly disparate genetic loci, ADSL loss-of-function variants and *KCTD13*, has provided a potential foothold to understand how purine signaling might influence autistic characteristics and highlights a new drug target and biomarker to further understand, treat, and diagnose autism.

Limitations of the study

- We could not clarify if S-Ado has a functional effect on neurons in this study or if inhibition of ADSS could reverse any functional deficits caused by elevated S-Ado. Further studies examining the effect of S-Ado on neurons would help clarify its role in several disease contexts such as 16p11.2 deletion syndrome and ADSL deficiency.
- Our data suggest a connection between 16p11.2 deletion syndrome and ADSL deficiency. Support for this connection could be obtained by showing S-Ado is elevated in the following: human 16p11.2 deletion syndrome iPSC (induced pluripotent stem cell)-derived neurons, the 16p11.2 mouse model or in serum, CSF or urine from patients with 16p11.2 deletions. Furthermore, showing that inhibition of ADSS would improve any phenotypes associated with 16p11.2 models would help support this connection.

Resource availability

Lead contact

Further information and requests for resources and reagents should be directed to and will be fulfilled by the Lead Contact, Jon M. Madison (jmadison@broadinstitute.org)

Materials availability

Plasmids generated in this study will be deposited to Addgene upon acceptance of this paper.

Sperm from the *Kctd13*$^{-}$ mouse line has been cryopreserved at the Jackson Laboratory, Bar Harbor, Maine and will be made publicly available upon acceptance of this manuscript.

Data and code availability

The original mass spectra may be downloaded from MassIVE (http://massive.ucsd.edu/) using the identifier: MSV000085846. The data are directly accessible via ftp://massive.ucsd.edu/MSV000085846/.

Methods

All methods can be found in the accompanying Transparent methods supplemental file.

Supplemental information

Supplemental Information can be found online at https://doi.org/10.1016/j.isci.2020.101935.

Acknowledgments

We thank members of the Stanley Center and the Stanley Center Therapeutics Group for helpful discussions and critical reading of the manuscript. A special thanks to the Broad vivarium staff for the maintenance and care of the animals used in this work. We thank Gil Prive for suggestions on the KCTD13 structural mutations. This work was supported by the Stanley Center for Psychiatric Research.

Author contributions

Conceptualization – J.M.M., E.M.S., and J.R.C.; Methodology – J.M.M., E.F.V., N.D.U., S.R.C., C.B.C., K.A.P., E.M.S., and J.R.C.; Investigation – J.M.M., K.D., E.R., S.F., N.D.U. M.C.L., A.S.G., E.F.V., and

K.A.P.; Variant selection – J.M.M., S.I., A.J.C., D.L., and F.W.; Resources – R.J.P. and F.Z.; Writing – original draft – J.M.M.; Writing – review and editing, J.M.M., K.D., E.F.V., N.D.U., S.A.C., J.R.C., and M.S.; Supervision – J.M.M, E.M.S., J.R.C., C.C., S.A.C, and C.B.C.

Declaration of interests

J.M.M. and A.J.C. are inventors on pending U.S. Patent Application No. 16/843,790, which is owned by the Broad Institute and is directed to certain subject matter disclosed herein.

Received: August 5, 2020
Revised: October 30, 2020
Accepted: December 8, 2020
Published: January 22, 2021

References

Baresova, V., Skopova, V., Sikora, J., Patterson, D., Sovova, J., Zikanova, M., and Kmoch, S. (2012). Mutations of ATIC and ADSL affect purinosome assembly in cultured skin fibroblasts from patients with AICA-ribosiduria and ADSL deficiency. Hum. Mol. Genet. *21*, 1534–1543.

Bennett, E.J., Rush, J., Gygi, S.P., and Harper, J.W. (2010). Dynamics of cullin-RING ubiquitin ligase network revealed by systematic quantitative proteomics. Cell *143*, 951–965.

Chen, Y., Yang, Z., Meng, M., Zhao, Y., Dong, N., Yan, H., Liu, L., Ding, M., Peng, H.B., and Shao, F. (2009). Cullin mediates degradation of RhoA through evolutionarily conserved BTB adaptors to control actin cytoskeleton structure and cell movement. Mol. Cell *35*, 841–855.

Deshpande, A., Yadav, S., Dao, D.Q., Wu, Z.Y., Hokanson, K.C., Cahill, M.K., Wiita, A.P., Jan, Y.N., Ullian, E.M., and Weiss, L.A. (2017). Cellular phenotypes in human iPSC-derived neurons from a genetic model of autism spectrum disorder. Cell Rep. *21*, 2678–2687.

Escamilla, C.O., Filonova, I., Walker, A.K., Xuan, Z.X., Holehonnur, R., Espinosa, F., Liu, S., Thyme, S.B., Lopez-Garcia, I.A., Mendoza, D.B., et al. (2017). Kctd13 deletion reduces synaptic transmission via increased RhoA. Nature *551*, 227–231.

Gitiaux, C., Ceballos-Picot, I., Marie, S., Valayannopoulos, V., Rio, M., Verrieres, S., Benoist, J.F., Vincent, M.F., Desguerre, I., and Bahi-Buisson, N. (2009). Misleading behavioural phenotype with adenylosuccinate lyase deficiency. Eur. J. Hum. Genet. *17*, 133–136.

Gooding, J.R., Jensen, M.V., Dai, X., Wenner, B.R., Lu, D., Arumugam, R., Ferdaoussi, M., MacDonald, P.E., and Newgard, C.B. (2015). Adenylosuccinate is an insulin secretagogue derived from glucose-induced purine metabolism. Cell Rep. *13*, 157–167.

Hodges, H., Fealko, C., and Soares, N. (2020). Autism spectrum disorder: definition, epidemiology, causes, and clinical evaluation. Transl. Pediatr. *9*, S55–S65.

Jurecka, A., Zikanova, M., Kmoch, S., and Tylki-Szymanska, A. (2015). Adenylosuccinate lyase deficiency. J. Inherit. Metab. Dis. *38*, 231–242.

Karczewski, K.J., Francioli, L.C., Tiao, G., Cummings, B.B., Alföldi, J., Wang, Q., Collins, R.L., Laricchia, K.M., Ganna, A., Birnbaum, D.P., et al. (2020). The mutational constraint spectrum quantified from variation in 141,456 humans. bioRxiv531210.

Lin, G.N., Corominas, R., Lemmens, I., Yang, X., Tavernier, J., Hill, D.E., Vidal, M., Sebat, J., and Iakoucheva, L.M. (2015). Spatiotemporal 16p11.2 protein network implicates cortical late mid-fetal brain development and KCTD13-Cul3-RhoA pathway in psychiatric diseases. Neuron *85*, 742–754.

Lydeard, J.R., Schulman, B.A., and Harper, J.W. (2013). Building and remodelling Cullin-RING E3 ubiquitin ligases. EMBO Rep. *14*, 1050–1061.

O'Roak, B.J., Vives, L., Girirajan, S., Karakoc, E., Krumm, N., Coe, B.P., Levy, R., Ko, A., Lee, C., Smith, J.D., et al. (2012). Sporadic autism exomes reveal a highly interconnected protein network of de novo mutations. Nature *485*, 246–250.

Portmann, T., Yang, M., Mao, R., Panagiotakos, G., Ellegood, J., Dolen, G., Bader, P.L., Grueter, B.A., Goold, C., Fisher, E., et al. (2014). Behavioral abnormalities and circuit defects in the basal ganglia of a mouse model of 16p11.2 deletion syndrome. Cell Rep. *7*, 1077–1092.

Sanders, S.J., Ercan-Sencicek, A.G., Hus, V., Luo, R., Murtha, M.T., Moreno-De-Luca, D., Chu, S.H., Moreau, M.P., Gupta, A.R., Thomson, S.A., et al. (2011). Multiple recurrent de novo CNVs, including duplications of the 7q11.23 Williams syndrome region, are strongly associated with autism. Neuron *70*, 863–885.

Sanders, S.J., He, X., Willsey, A.J., Ercan-Sencicek, A.G., Samocha, K.E., Cicek, A.E., Murtha, M.T., Bal, V.H., Bishop, S.L., Dong, S., et al. (2015). Insights into autism spectrum disorder genomic architecture and biology from 71 risk loci. Neuron *87*, 1215–1233.

Schizophrenia Working Group of the Psychiatric Genomics, C (2014). Biological insights from 108 schizophrenia-associated genetic loci. Nature *511*, 421–427.

Stayton, M.M., Rudolph, F.B., and Fromm, H.J. (1983). Regulation, genetics, and properties of adenylosuccinate synthetase: a review. Curr. Top Cell Regul. *22*, 103–141.

Stessman, H.A., Xiong, B., Coe, B.P., Wang, T., Hoekzema, K., Fenckova, M., Kvarnung, M., Gerdts, J., Trinh, S., Cosemans, N., et al. (2017). Targeted sequencing identifies 91 neurodevelopmental-disorder risk genes with autism and developmental-disability biases. Nat. Genet. *49*, 515–526.

Takumi, T., and Tamada, K. (2018). CNV biology in neurodevelopmental disorders. Curr. Opin. Neurobiol. *48*, 183–192.

Teng, X., Aouacheria, A., Lionnard, L., Metz, K.A., Soane, L., Kamiya, A., and Hardwick, J.M. (2019). KCTD: a new gene family involved in neurodevelopmental and neuropsychiatric disorders. CNS Neurosci. Ther. *25*, 887–902.

Traynelis, J., Silk, M., Wang, Q., Berkovic, S.F., Liu, L., Ascher, D.B., Balding, D.J., and Petrovski, S. (2017). Optimizing genomic medicine in epilepsy through a gene-customized approach to missense variant interpretation. Genome Res. *27*, 1715–1729.

Tyagi, A.K., and Cooney, D.A. (1980). Identification of the antimetabolite of L-alanosine, L-alanosyl-5-amino-4-imidazolecarboxylic acid ribonucleotide, in tumors and assessment of its inhibition of adenylosuccinate synthetase. Cancer Res. *40*, 4390–4397.

Udeshi, N.D., Mertins, P., Svinkina, T., and Carr, S.A. (2013). Large-scale identification of ubiquitination sites by mass spectrometry. Nat. Protoc. *8*, 1950–1960.

Wang, T., Guo, H., Xiong, B., Stessman, H.A., Wu, H., Coe, B.P., Turner, T.N., Liu, Y., Zhao, W., Hoekzema, K., et al. (2016). De novo genic mutations among a Chinese autism spectrum disorder cohort. Nat. Commun. *7*, 13316.

Yuen, R.K., Merico, D., Bookman, M., J, L.H., Thiruvahindrapuram, B., Patel, R.V., Whitney, J., Deflaux, N., Bingham, J., Wang, Z., et al. (2017). Whole genome sequencing resource identifies 18 new candidate genes for autism spectrum disorder. Nat. Neurosci. *20*, 602–611.

Zheng, N., and Shabek, N. (2017). Ubiquitin ligases: structure, function, and regulation. Annu. Rev. Biochem. *86*, 129–157.

Zikanova, M., Skopova, V., Hnizda, A., Krijt, J., and Kmoch, S. (2010). Biochemical and structural analysis of 14 mutant adsl enzyme complexes and correlation to phenotypic heterogeneity of adenylosuccinate lyase deficiency. Hum. Mutat. *31*, 445–455.

iScience, Volume *24*

Supplemental Information

Regulation of purine metabolism connects KCTD13 to a metabolic disorder with autistic features

Jon M. Madison, Karen Duong, Ellen F. Vieux, Namrata D. Udeshi, Sumaiya Iqbal, Elise Requadt, Shaunt Fereshetian, Michael C. Lewis, Antonio S. Gomes, Kerry A. Pierce, Randall J. Platt, Feng Zhang, Arthur J. Campbell, Dennis Lal, Florence F. Wagner, Clary B. Clish, Steven A. Carr, Morgan Sheng, Edward M. Scolnick, and Jeffrey R. Cottrell

MTR viewer plot for KCTD13

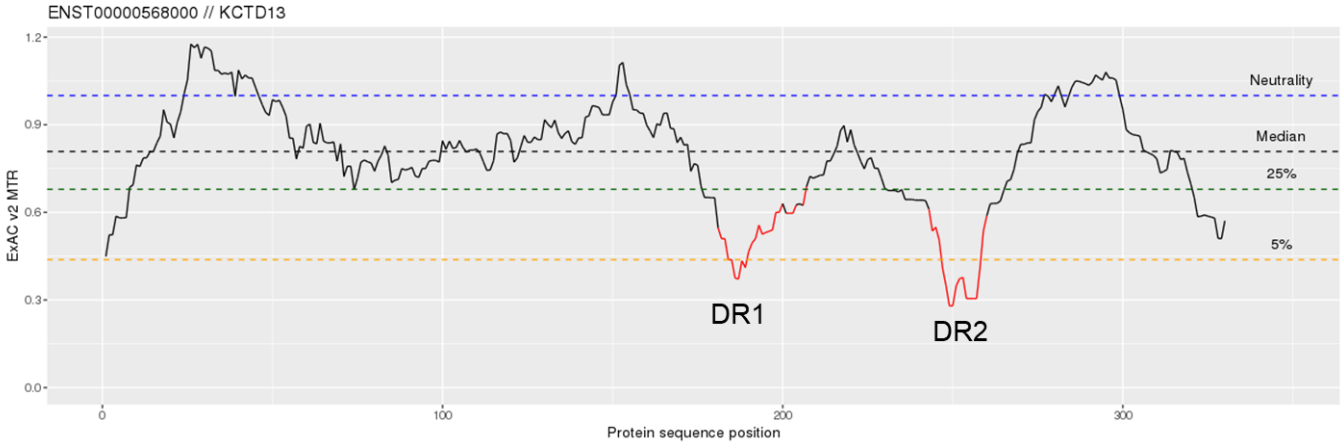

Figure S1, Related to Figure 4. MTR Viewer plot for KCTD13. The Missense Tolerance Ratio plot for KCTD13 is shown. The two regions labeled DR1 and DR2 are indicated on the plot. These regions correspond to the regions analyzed in Figure 4.

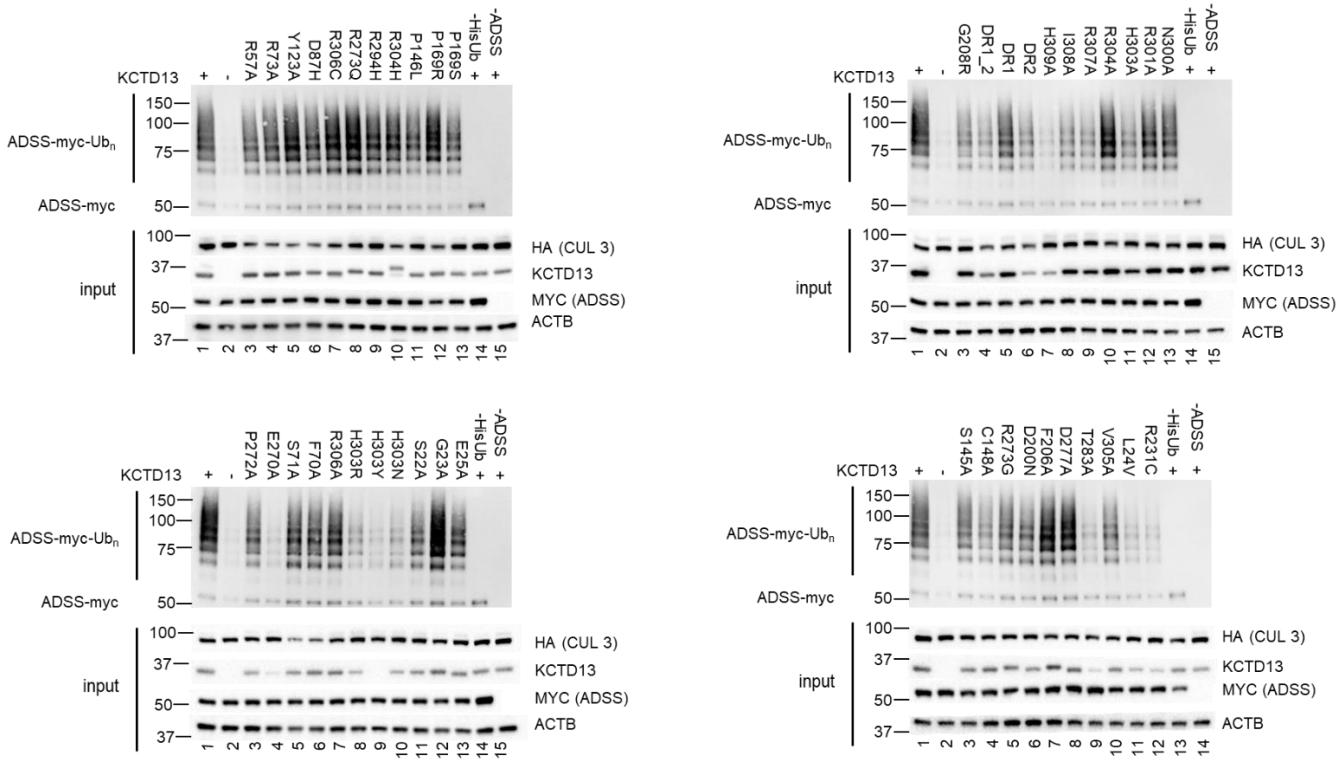

Figure S2, Related to Figure 4. Specific KCTD13 mutations alter ADSS ubiquitination. *ADSS-myc*, *KCTD13* (WT and mutant plasmids), *HA-CUL3*, *RBX1* and *6xhistidine ubiquitin* plasmids were transfected into HEK cells in the combinations indicated. His-ubiquitin tagged conjugated proteins were collected under denaturing conditions using Ni-NTA magnetic beads. Proteins were eluted from the beads and western transfer was performed. Membranes were probed with a myc antibody to determine if ADSS-myc had been ubiquitinated. Total whole cell lysates were isolated and a western transfer was performed and blotted with the indicated antibodies to verify the expression of the indicated proteins. These data suggest ADSS ubiquitination is altered by DNA variation in KCTD13.

Transparent Methods

EXPERIMENTAL MODELS AND SUBJECT DETAILS

KCTD13 mouse lines and timed pregnancies

All care and maintenance of mice were carried out in accordance with NIH and Broad Institute IACUC guidelines. As described in Method Details, ddPCR was used to determine the genotype of animals used for KCTD13 E18 dissociated neuronal cultures. Timed pregnancies were set up by Broad Institute Vivarium staff and timed from the identification of vaginal plugs in females. Identification of a vaginal plug was considered day 0.5 and embryos were collected on day 18. Sperm from this *Kctd13*$^{-}$ mouse model was cryopreserved at Jackson Laboratories and will be made available to the public.

Cell Culture

Primary neuron cell culture

The dissociation and growth of primary embryonic day 18 mouse neuronal cultures is described in detail in the method details. Primary neurons were grown in NBActive4 media (Brain Bits) on poly-D-lysine plates in 5% CO2 at 37°C. Unless otherwise noted, cultures were grown for 21 days from the date of dissection until they were collected for experimental analysis. Media was not changed during the course of the 21 days *in vitro*. Neuronal cultures were maintained antibiotic free.

Mammalian cell lines

HEK 293T cells were obtained from ATCC and grown in DMEM (Gibco) supplemented with 10% Fetal bovine serum albumin (Gibco) at 37°C in 5% CO2. Cultures were regularly tested for mycoplasma using a luminescence assay (Lonza) and were found to be mycoplasma free. Cultures were maintained antibiotic free.

METHOD DETAILS

Antibodies

Myc-tag Rabbit mAb (CST 71D10-2278S)**,** KCTD13 Rabbit (Pr2905)**,** HA-tag Rabbit mAb (CST C29F4-3724S)**,** IgG Rabbit polyclonal ChIP Grade 0.2mg/mL (ab27478)**,** V5-tag Rabbit mAb (CST D3H8Q-13202S)**,** Myc-tag Mouse mAb (CST 9B11-2276S)**,** KCTD13 (B-12) Mouse monoclonal IgG 200μg/mL (sc-393994)**,** KCTD13 Rabbit polyclonal Ab (21st Century Biochemicals, Pr2905) (see description below), HA-tag Mouse mAb (CST 6E2-2376S)**,** Anti-V5 Antibody Mouse monoclonal 50μL at 1.01mg/mL (Invitrogen P/N 46-0705)**,** B-Actin Rabbit mAb (HRP Conjugate) (CST D6A8-12620S)**.**

Plasmids

pCMV6 *hADSS*-myc-flag (Origene: RC204256), V82 *hKCTD13*_IRESPuro, V17 *hCUL3-HA-Flag*_IRESPuro, V20 *hRBX1*_IRESPuro, *His-ubiquitin* (WB Kailin, Dana-Farber Institute, Harvard Medical School).

Animal care and maintenance

All care and maintenance of mice were carried out in accordance with NIH and Broad Institute IACUC guidelines.

Dissociated neuronal cultures

Time pregnancies were generated from WT x WT and *Kctd13*$^{-/-}$ x *Kctd13*$^{-/-}$ matings. The sex of the embryos was not determined. Timed pregnant females were euthanized following Broad IACUC approved methods. E18 embryos were collected and rapidly decapitated. Embryos were then washed in dissection media (Hibernate-E (Hib-E, Gibco) supplemented with 100U/mL penicillin streptomycin (Pen/Strep, Gibco)). Brains were isolated, cortices were separated from

the midbrain and meninges were removed from each cortex. These forebrains (hippocampus, striatum, and cortex) were cut into six pieces; five forebrains were pooled for dissociation. To dissociate 5 forebrains, one Papain kit (Worthington LK3176) was reconstituted in 5mLs Hib-E and activated at 37°C for 10 minutes. Following activation, DNase I (Sigma, DN25) was added to a concentration of 10µg/mL and filter sterilized using a 0.22µm filter. Forebrains were washed twice with 5mLs of Hib-E and 5mLs of activated papain/DNase I was added to the forebrains and incubated for 8 minutes at 37°C. Following digestion, forebrains were washed three times with 10mLs Hib-E per wash. Forebrains were then triturated 10-15 times with a P1000 pipette in 1 mL NBActive4 supplemented with 10 µg/mL DNAse I filter sterilized using a 0.22 µm filter. The cell mixture was then allowed to settle for 1 minute at room temperature (RT) and the supernatant was transferred to a new tube containing 4mLs of NBActive4 media and spun at 1000 RPM for 5 minutes at RT. The supernatant was aspirated and the pellet was gently resuspended in 1mL NBActive4 media. Cells were counted in a hemocytometer, diluted and plated at 1 million cells/well in a 6-well pol-D-lysine coated plate (Corning, Biocoat) or 6 million cells/10cm poly-D-lysine coated plate (Corning, Biocoat).

For western blots neurons were collected in urea lysis buffer [8 M Urea (Sigma), 75 mM NaCl (Sigma), 1 mM EDTA (Sigma), 50 mM Tris pH 8.0 (Sigma), 1:100 PIC2 (Sigma), 1:100 PIC3 (Sigma), 0.1 mM Chloroacetamide (Sigma), 10 mM NaF (Sigma), 2mM PMSF (Aldrich), Roche protease inhibitor mini (Roche), 50µM PR-619 (Lifesensors), 1,10 orthophenanthroline (Sigma)] by scraping. For SDS-PAGE and Western blots, Laemmli buffer was added to samples, they were boiled, and a sample was run on a 4-12% Bis-Tris SDS PAGE gel and transferred to a nitrocellulose membrane.

Co-Immunoprecipitation

For transfections, 7.6 million 293T HEK cells were plated in a 10 cM tissue culture dish 24 hours in advance of transfection. Cells were transfected according to manufacturer's instructions using Lipofectamine 2000 (Invitrogen) and Opti-MEM (Gibco). Cells were collected 72 hours post-transfection after media was aspirated, cells were washed 1X with chilled PBS, collected in 10 mLs chilled PBS, centrifuged (1000 RPM, 5 min, 4°C). Supernatant was aspirated and pellets were snap frozen in liquid nitrogen. Pellets were stored at -80°C until processed. Cell pellets were lysed with 1mL ubiquitin lysis buffer (1X CST lysis buffer (Cell Signaling Technology), 1:100 PIC2 (Sigma), 1:100 PIC3 (Sigma), 0.1 mM chloracetamide (Sigma), 10 mM NaF (Sigma), 2mM PMSF (Aldrich), Roche protease inhibitor mini (Roche), 50 μM PR-619 (LIfesensors), 1,10 orthophenanthroline (Sigma)). Prior to collecting antibody protein complexes, protein A magnetic Dynabeads (Thermo-Fisher/Invitrogen) were blocked in 5% BSA for 1 hour with rocking at 4°C. Dynabeads were then loaded with 1μg CHIP grade IgG (Abcam) with rocking at 4°C for 1 hour and then 50 μL of beads were added to the protein lysates to preclear of any nonspecific IgG-Dynabead binding proteins. Whole cell lysates were prepared from frozen pellets by sonicating pellets resuspended in 1mL ubiquitin lysis buffer in a Diagenode water bath sonicator on HIGH for 5 minutes at 4°C. Lysates were spun at 14 KRPM for 10 minutes at 4°C. Supernatant were transferred to a new tube and 50 μL of a 50% slurry of pre-loaded, pre-blocked beads were added to the lysate for 1 hour at 4 °C with rocking. Beads were collected using a magnet and supernatant was transferred to a clean tube. Lysate was divided among 8 aliquots (125 μL) and primary antibody against myc epitope (CST, clone 71D10) (rb) or KCTD13 (see KCTD13 antibody production) or rabbit IgG was added at a 1:50 (i.e., 2.5 μL) dilution. Lysates were rocked at 4 °C for 1 hour. While antibody-lysate mixtures were rocking, a fresh 50% slurry of protein-A magnetic Dynabeads was prepared in ubiquitin lysis buffer (50% bead slurry). Beads were washed and resuspended as described previously. At the end of 1 hour, 50 μL of bead slurry was added to each protein antibody mixture to collect antibody protein immunocomplexes. Following collection

of immunocomplexes, beads were washed 5 times with 0.5 mL RIPA wash buffer (10 mM Tris-Cl, pH 8.0, 1mM EDTA, 1% Triton X-100, 0.1% sodium deoxycholate, 0.1% SDS, 140 mM NaCl) supplemented with 2mM PMSF and 1X Roche protease inhibitor cocktail (Roche). After each addition of RIPA wash buffer, beads were collected using a magnet. After the final wash step buffer was completely aspirated to ensure all wash buffer was completely removed. Beads were resuspended in 75 μL of 2X Laemmli buffer (BioRad) containing 0.7 M beta-mercaptoethanol (BME, Sigma) to elute proteins. Samples were then heated at 95 °C for 6 minutes to denature proteins and either western blots were run as described below or samples were stored at -80 °C. To measure the input levels of transfected proteins in whole cell lysates, 50 μL of starting lysate was mixed with 48 μL 4X Laemmli buffer plus 2 μL BME and heated at 95 °C for 6 minutes. When necessary, lysates were further diluted with 2X Laemmli buffer. Western transfers and immunoblotting were carried out using the Thermo-Fisher/Invitrogen Bolt system Briefly, 5 μL of each eluted IP sample was loaded on an 8% Bolt Bis-Tris-Plus Gel (15-well) and run in Bolt 1X MOPS Running buffer (BOLT). Gels were run at 165V for 32 minutes and transferred using an iBLOT2 to nitrocellulose for 7 minutes. Following western transfer, membranes were blocked in 5% BSA in 1X Tris Buffered Saline plus Tween (TBS-T, Sigma) for 1 hour at RT on a rocking platform. Following blocking, primary antibody (Myc or KCTD13) was added at 1:1000 and incubated on a rocking platform at 4°C overnight. Subsequently, membranes were washed with 3 brief washes to remove the antibody mixture, followed by three washes with 1X TBS-T for 5 minutes each. Secondary antibody consisting of donkey anti rabbit conjugated to horseradish peroxidase (GE Healthcare, NA934) diluted 1:5000 in 5% blotting milk (Bio-Rad) in TBS-T was then added to membranes and incubated at RT for 1 hour on a rocking platform. Membranes were washed with 3 brief washes to remove the antibody mixture, followed by three washes with 1X TBS-T for 5 minutes each. Just prior to imaging, the membranes were rinsed once with Tris-Buffered Saline without Tween. Membranes were incubating in Femto ECL (Pierce) for 1 minute

and then imaging on a Bio-Rad Chemidoc. For loading controls for input levels of proteins, membranes were incubated with an antibody to B-actin coupled to HRP (Cell Signaling Technology) diluted in 5% BSA in TBS-T for 1 hour followed by washing as described for other primary and secondary antibodies.

Kctd13 deletion mouse generation

CRISPR/Cas9 system guide RNAs targeting the first exon of *Kctd13* were used to create a deletion in exon 1 of the mouse *Kctd13* gene as described below.

In vitro validation of sgRNAs

The sgRNA, gccggctgcggccgaatgct**,** that was used to create the Kctd13 mouse was designed using the CRISPRtool (crispr.mit.edu). To validate sgRNA targeting of the *Kctd13* locus, U6-sgRNA PCR products were generated using Herculase II DNA polymerase (Agilent), purified using QIAquick PCR Purification Kit (Qiagen), and co-transfected with a Cas9 expression plasmid into mouse N2a cells (ATCC) using Lipofectamine 2000 (Life Technologies). Three days after transfection, genomic DNA was extracted with QuickExtract DNA Extraction Solution (Epicenter) and used as a template for PCR amplification with Herculase II DNA polymerase (Agilent). PCR amplicons were purified, and 200 ng was used as an input into the SURVEYOR assay (Transgenomic), run on a 2% E-gel (Life Technologies), and quantified using relative band intensities.

Preparation of Cas9 mRNA and sgRNA RNA for zygote injection

Human codon optimized Cas9 (from *Streptococcus pyogenes*) capped and polyadenylated mRNA was prepared by *in vitro* transcription using mMessage mMachine T7 ULTRA Transcription Kit (Ambion). sgRNA RNA was prepared by *in vitro* transcription using Megashortscript T7 Transcription Kit (Ambion) with an annealed partially double stranded

template. Both Cas9 mRNA and sgRNA RNA were purified by MEGAclear Transcription Clean-Up Kit (Ambion) and mixed to a final concentration of 200 ng/μL Cas9 mRNA and 50 ng/μL sgRNA RNA in H_2O for injection.

Generation of germline mutant mice

Three-five week old C57BL/6N (Taconic) female mice (superovulation and plugged 0.5 dpc) were used as zygote donors and CD-1(ICR) females were used as foster mothers. Three days prior to zygote injections, pregnant mare's serum (PMS) 5 IU was administered IP to each donor female. Forty-seven hours later hCG 5 IU was administered by IP injection and then females were paired with stud males. Donor females were sacrificed 0.5 pcd and ovaducts were collected and placed into 0.1% hyaluronidase/flushing holding media (FHM) (Millipore). Using two pairs of forceps the swollen ampulla was torn open releasing the eggs/cumulus cell bunch. The zygotes were washed in drops of FHM and the cumulus cells were removed and put into KSOM-aa culture medium (Millipore) for an hour before injection. 5 μL of Cas9/sgRNA RNA mixture was loaded into a microinjection needle (prepared by Needle puller Sutter P-97) and attached to the microinjector (Eppendorf microinjector 5242). Sets of eggs were placed into 100 μL FHM drops covered with mineral oil at RT. The larger pronucleus was injected until an obvious expansion occurred. Eggs were placed back into the warm and equilibrated KSOM-aa culture medium and incubated overnight. 12 hours later the two-cell stage embryos were surgically implanted bilaterally into the oviducts of 0.5 dpc CD-1 recipients. A maximum of 26 two-cell embryos were transferred into one recipient and monitored for pregnancy. To identify progeny that contained indels in the targeted *Kctd13* exon, the genotyping primers *Kctd13* primer1 For: cggagtagctgtggagagtgg and *Kctd13* primer2 Rev: aaggattggggaaagagagagatt, were used.

The reverse primers for U6-sgRNA PCR product production were:

Primer1

AAAAAAAGCACCGACTCGGTGCCACTTTTTCAAGTTGATAAcggactagccttattttaacttgCTATTTCT

AGCTCTAAAACagcattcggccgcagccggcggtgTTTCGTCCTTTCCACaag

Primer2

AAAAAAAGCACCGACTCGGTGCCACTTTTTCAAGTTGATAAcggactagccttattttaacttgCTATTTCTAGC

TCTAAAACtcgtacagtctgaagcccctCggtgTTTCGTCCTTTCCACaag

Primer3

AAAAAAAGCACCGACTCGGTGCCACTTTTTCAAGTTGATAAcggactagccttattttaacttgCTATTTCTAGC

TCTAAAACtgagggtgcgcagcgtggtgCggtgTTTCGTCCTTTCCACaag

The reverse primers for sgRNA IVT were:

IVT primer1:

aaaaaagcaccgactcggtgccacttttttcaagttgataacggactagccttattttaacttgctatttctagctctaaaacagcattcggc

cgcagccggccctatagtgagtcgtatta

IVT primer2:

aaaaaagcaccgactcggtgccacttttttcaagttgataacggactagccttattttaacttgctatttctagctctaaaactcgtacagtct

gaagcccctccctatagtgagtcgtatta

IVT primer3

aaaaaagcaccgactcggtgccacttttttcaagttgataacggactagccttattttaacttgctatttctagctctaaaactgagggtgcg

cagcgtggtgccctatagtgagtcgtatta

Genotyping *Kctd13* mice

During the course of working with the *Kctd13*$^{-}$ mice we discovered amplification bias made genotyping heterozygote *Kctd13*$^{-}$mice difficult. We therefor designed a primer pair and probe suitable for droplet digital PCR (ddPCR) that allowed us to accurately genotype all allelic combinations of the *Kctd13*$^{-}$ allele. The genotyping primers were: *Kctd13* F 47_64nt (TCC GCT CAC TGG CAT GTC), *Kctd13* R 47_64nt (CAC ACT CGA GGG GCT AGG), *Kctd13* 47_64nt

probe (/56-FAM/TGC GGC CGA /ZEN/ATG CTT GGA GTC C/3IABkFQ/). To genotype mice genomic DNA from either ear clip or tail clips was obtained by adding 75 μL of 25 mM NaOH, 0.2 mM EDTA to the tissue and incubating for 30 minutes at 95 °C followed by neutralization with 75 μL 40 mM Tris-HCl pH 5. Genotyping was carried out by mixing 1 μL of the genomic DNA mixture with the ddPCR assay and 1X ddPCR mix for Probes (Bio-Rad). Droplets were prepared according to the manufacturer's instructions in a Bio-Rad Droplet generator. Droplets were cycled according to the manufacturer's instructions. Following cycling, droplets were counted in an X100 ddPCR instrument (Bio-Rad). Bio-Rad ddPCR Quantasoft software was used to determine the DNA content of each sample/genotype of each mouse.

Antibody generation

A peptide specific antibody was generated against the c-terminal peptide CVRRHITHDERPHGQQIVFKD-OH of KCTD13. This peptide was injected into two New Zealand white rabbits (Dana-Farber Institute, 21st Century Biochemicals). The resulting serum was affinity purified against the same peptide and eluted into PBS. This polyclonal antibody, Pr2905, was used at a dilution of 1:1000 for western blots and 1:50 for immunoprecipitations.

HEK *in cell* reconstitution of ADSS ubiquitination

A day before transfection (day -1) 293T HEK (HEK) cells were plated in 10 cm dishes at 7.6-8 million cells per dish. The next day (day 0), the plasmids containing His-Ubiquitin (Gift of Dr. WG Kaelin, Harvard Medical School), *KCTD13*, *HA-CUL3* and *ADSS-myc* were transfected into HEK cells. Two days following transfection, bortezomib was added to the transfected cells to a final concentration of 2 μM. After 5 hours cells were harvested into PBS by scraping. 1 mL of the cell suspension was transferred to a tube for use as transfection controls and spun at 2500 RPM at 4°C. The remaining 9 mLs were transferred to a 15 mL Falcon tube and spun at 1K for 5 minutes

at 4°C. The supernatant was removed. The cell pellets were then frozen in liquid N2. Samples were stored at -80°C until ready to proceed with immunoprecipitation. For pulldowns, cell pellets were resuspended in 1 mL of chilled (4°C) Buffer C (6M Guanidine-HCl, 0.1M $NaPO_4$, 10 mM Imidazole) then sonicated (Branson sonicator, microtip, power 30%, cycle 50, 10 to 15 pulses). Buffer C equilibrated Ni-NTA magnetic beads (Invitrogen) were added to the sonicated lysate. Beads were incubated for 2 hours at 4 °C with rocking to collect His-Ub conjugated proteins. Beads were then washed twice with Buffer C supplemented with 2 mM PMSF, 1x Roche Protease inhibitors, twice with Buffer D (1:3 volume ratio Buffer C:Buffer E), once with Buffer E (25 mM Tris-Cl, pH 6.8, 20 mM imidazole, protease inhibitor (Roche), 2 mM PMSF). Bound proteins were then eluted by boiling in 300 mM imidazole, 2X Laemmli PAGE buffer, 0.7M BME. Eluted samples were loaded on a 4-12% Bolt Bis-Tris PAGE gel (Invitrogen) and run in MOPS buffer. A western transfer was performed and probed with the appropriate primary and secondary antibodies.

For transfection controls, cell pellets were resuspended in 100 μl of CST lysis buffer or RIPA buffer, 2 mM PMSF and 1X protease inhibitor tablet (Roche) and sonicated with a Diagenode water bath sonicator for 10 minutes. Samples were spun at 4°C for 10 minutes, 12,000 RPM and supernatant was transferred to a new tube. An equal volume of 4X gel loading dye + 0.7M BME was added and the samples were boiled for 10 minutes. Samples were Western blotted with the appropriate primary and secondary antibodies.

SILAC labeling of mouse primary neurons

Forebrains (cortex, hippocampus and striatum) were dissected from either wild-type C57B6 or *Kctd13*$^{-}$C57B6. E18 timed pregnant females were euthanized using Broad IACUC approved methods. Neurons were dissected and dissociated using papain as described above. Neurons were plated on 10 cM poly-D-lysine coated plates at a density of 6 million cells per plate in either heavy or light SILAC media. Neurons were fed every other day for 21 days *in vitro*. This feeding

schedule resulted in greater than 95% labeling of cells. Neurons were then scraped into ubiquitin lysis buffer. Plates of a common genotype and metabolic labeling state were pooled for further processing. SILAC labels were flipped for each genotype. K-ε-GG and total proteome profiling were later performed for both replicates

Cell lysis and trypsin digestion for K-ε-GG and proteome profiling

SILAC-labeled neurons were lysed on plates by washing once with 10 mLs ice cold PBS and then scraping into 350 μL of ice cold urea lysis buffer (8 M urea, 50 mM Tris-HCl, pH 7.5, 150 mM NaCl, 1 mM EDTA, 2 μg/mL Aprotinin (Sigma-Aldrich), 10 μg/mL leupeptin (Roche Applied Science), 1 mM phenylmethylsulfonyl fluoride (PMSF), 50 μM PR-619, and 1 mM chloroacetamide). Plates of a common genotype and label were pooled for processing. Following lysis, samples were centrifuged at 20,000 x g for 15 minutes at 4 °C to remove insoluble material. Protein concentrations were determined using a bicinchoninic acid (BCA) protein assay (Pierce) and samples were mixed equitably per SILAC state. Proteins were reduced with 5 mM dithiothreitol for 45 minutes at RT and subsequently carbamidomethylated with 10 mM iodoacetamide for 30 minutes at RT in the dark. Samples were diluted to 2 M urea with 50 mM Tris-HCl, pH 7.5, and digested with sequencing grade trypsin (Promega) at 25°C overnight using an enzyme to substrate ratio of 1:50. Digested samples were acidified to 1% formic acid (FA) (Sigma-Aldrich). Tryptic peptides were desalted on 500-mg tC18 Sep-Pak SPE cartridges (Waters). Cartridges were conditioned with 5 mLs of 100% acetonitrile (MeCN), 5 mL of 50% MeCN/0.1% FA, and four times with 5 mLs of 0.1% trifluoroacetic acid (TFA). Up to 15 mg of sample was loaded onto a single cartridge, and subsequently washed 3 times with 5 mL of 0.1% TFA. Samples were eluted from cartridges by washing 2 times with 3 mLs of 50%MeCN/0.1%FA. Desalted samples were dried overnight in a Savant SC210A SpeedVac concentrator (Thermo Scientific).

Basic pH reverse phase fractionation

Offline basic pH reverse phase (bRP) fractionation was completed using a custom-manufactured Zorbax 300 Extend-C18 column (9.4 x 250 mm, 300 Å, 5 µm, Agilent) on an Agilent 1100 series HPLC system. Approximately 15 mg of peptide sample was resuspended in 1.8 mL of basic RP solvent A (2% MeCN, 5 mM ammonium formate, pH 10), separated into 2 HPLC vials and injected with Solvent A at flow rate of 3 mL/min. A 64-minute method was used for fractionation. The gradient was composed of an initial increase to 8% Solvent B (1.1% B/min) (90% MeCN, 5 mM ammonium formate), followed by a 38-minute linear phase (0.5% B/min) where the amount of solvent B was increased from 8% to 27% and ramp phases where the Solvent B amount was increased from 31% (1% B/min) to 39% (0.5% B/min), and finally to 60% (3%B/min). A total of 96 fractions of 2 mL each were collected every 0.66 minutes at a flow rate of 3 mL/min. For the proteome profiling, 5% of each fraction was pooled into 22 fractions. For ubiquitination profiling, 95% of each fraction was pooled into 8 fractions using a concatenated pooling strategy. Pooled samples were dried using a SpeedVac concentrator.

Ubiquitinated peptide enrichment

The anti-K-ε-GG antibody was obtained from the PTMScan® ubiquitin remnant motif (K-ε-GG) kit (Cell Signaling Technology). Prior to enrichment, the antibody was covalently coupled to Protein A agarose beads by chemical cross-linking with dimethyl pimelimidate (DMP). For cross-linking, the antibody bound beads were first washed three times with 1 mL of 100 mM sodium borate, pH 9 and then incubated in 1 mL of 20mM DMP for 30 minutes with rotation at RT. The reaction was stopped by washing beads twice with 1 mL of 200 mM ethanolamine, pH 8 followed by incubation for 2 hours at 4°C with rotation. Antibody-bound beads were washed three times in 1.5 mL of ice-cold immunoprecipitation (IAP) buffer (50 mM MOPS, pH 7.2, 10 mM sodium phosphate, 50 mM NaCl), resuspended in IAP buffer, and stored at 4°C. For K-ε-GG enrichment, bRP fractions were

reconstituted in 1.5 mLs of IAP buffer and each fraction was incubated with 32 μg of cross-linked anti- K-ε-GG antibody for 1 hour, at 4°C, while rotating. Following incubation, samples were spun down at 2000 x g and the supernatant was removed. Antibody-bound beads were washed 4X with 1.5 mLs of ice cold PBS and peptides were then eluted from the beads with 2 x 50µL of 0.15% TFA. Eluted peptides were desalted using C18 StageTips. Each StageTip was packed with two plugs of C18 material (EmporeTM C18 Extraction Disk; 3M) and then conditioned with 100 µL of MeOH, 100uL of 50% MeCN/0.1% FA, and twice with 100µL of 0.1% FA. K-ε-GG peptides were loaded onto the conditioned StageTips, washed twice with 100µL of 0.1% FA, eluted with 50 µL of 50% MeCN/0.1% FA, and dried to completeness.

LC-MS/MS analysis

K-ε-GG and global proteome fractions were reconstituted in 8 µL and 20 µL of 3% MeCN/1% FA, respectively, and analyzed by nanoflow-UPLC-HCD-MS/MS using a Q Exactive mass spectrometer (Thermo Fisher Scientific) coupled on-line to a Proxeon Easy-nLC 1000 system. 4µL and 1µL of K-ε- GG and global proteome samples were injected, respectively, for each analysis. Samples were injected onto a microcapillary column (360 µm OD x 75 µm ID) packed with 24 cm of ReproSil-Pur C18-AQ 1.9 µm beads (Dr. Maisch GmbH) that was equipped with an integrated electrospray emitter tip (10 µm). For online analyses, the column was heated to 50 C using a 20 cm column heater (Phoenix S&T). For LC separation, solvent A was 0.1 % FA/3 % MeCN and solvent B was 90% MeCN/0.1% FA. Peptides were eluted into the mass spectrometer at a flow rate of 200 nL/min using a gradient consisting of a linear phase at 0.3% B/min, followed by a ramp to 60% B (10% B/min). The total analysis time for each sample was 150 minutes. The Q Exactive instrument was operated in the data-dependent mode acquiring HCD MS/MS scans (R=17,500) after each MS1 scan (R=70,000) on the 12 top most abundant ions using an MS1 ion target of 3x 106 ions and an MS2 target of 5x104 ions. The maximum ion time utilized for the

MS/MS scans was 120 ms; the HCD-normalized collision energy was set to 25; the dynamic exclusion time was set to 20s, and the peptide match and isotope exclusion functions were enabled.

MS data analysis

MS data was analyzed with the MaxQuant software version 1.3.0.5 and searched against the mouse Uniprot database that contained 248 common laboratory contaminants was provided by the MaxQuant software package. The search parameters were as follows: enzyme specificity was set to trypsin, maximum number of mixed cleavages set to 2, precursor mass tolerance was at 20 ppm for the first search and set to 6 ppm for the main search. Oxidized methionine and N-terminal protein acetylation were searched as variable modifications, with carbamidomethylation of cysteines searched as a fixed modification. For searching K-ε-GG data files, Gly-Gly addition to lysine was also searched as a variable modification. The minimum peptide length was set to 6, and false discovery rate for peptide, protein, and site identification was set to 1%. The filter labeled amino acids and peptide quantification functions were enabled. For proteome data, proteins were considered if they were identified by 2 or more razor/unique peptides and quantified by 3 or more ratio counts in both biological replicates. For the ubiquitylome data, K-ε-GG sites were considered if they were confidently localized (>0.5) and quantified in both biological replicates. SILAC ratios for ubiquitiylation sites were normalized by corresponding proteome SILAC ratios. Differential protein and K-ε-GG site abundances between *Kctd13*$^{-/-}$ and *Kctd13* WT neurons were identified using a moderated *t*-test using Bland-Altman filtering with the limma R-package (Ritchie et al., 2015) implemented in Protigy. *P* values were adjusted for multiple hypothesis testing using the Benjamini–Hochberg method.

The original mass spectra for all experiments, and the protein sequence database used for searches have been deposited in the public proteomics repository MassIVE (https://massive.ucsd.edu) and are accessible at ftp://MSV000085846@massive.ucsd.edu with

username: MSV000085846, password: autistic. This dataset will be made public upon acceptance of the manuscript.

Metabolic profiling of neurons

For metabolite extraction, samples were collected from either cells or the cell media. Cell samples were extracted from cells grown in 12 well plates. Cell samples were extracted by washing cells once with 1 mL of ice-cold PBS, transferring to dry ice, followed by the addition of 400 μL of 80% methanol (VWR) containing the internal standards inosine-^{15}N4, thymine-d4, and glycocholate-d4 (Cambridge Isotope Laboratories). Cells were then incubated for 15 minutes at -80°C, followed by scraping and transfer of the methanol and cells to a 1.5 mL tube. Cells were centrifuged (10 minutes, 9,000 x *g*, 4°C), and the supernatant was transferred to a new 1.5mL tube. The pellet was extracted again using 50 μL of 80% methanol containing internal standards and centrifuged. The supernatant was then pooled with the previously collected methanol sample. Media supernatant samples (30 µL) were extracted using 120 µL of 80% methanol (VWR) containing the internal standards inosine-^{15}N4, thymine-d4, and glycocholate-d4 (Cambridge Isotope Laboratories). The samples were centrifuged (10 minutes, 9,000 x *g*, 4°C). The resulting supernatant was transferred to a new tube. Samples were stored at -80°C until analysis. A method using basic HILIC separation and negative ionization mode MS detection was established on an LC-MS system consisting of an ACQUITY UPLC (Waters Inc.) coupled to a 5500 QTRAP triple quadrupole mass spectrometer (AB SCIEX). Supernatants were injected directly onto a Luna NH2 column (150 × 2.0 mm, 5 µm particle size; Phenomenex) that was eluted at a flow rate of 400 µL/min with initial conditions of 10% mobile phase A (20 mM ammonium acetate and 20 mM ammonium hydroxide (Sigma-Aldrich) in water (VWR)) and 90% mobile phase B (10 mM ammonium hydroxide in 75:25 v/v acetonitrile/methanol (VWR)) followed by a 10-minute linear gradient to 100% mobile phase A. MS data were acquired using multiple reaction monitoring and

retention times, declustering potentials, and collision energies were determined using authentic reference standards. The ion spray voltage was −4.5 kV and the source temperature was 500°C.

Raw data were processed using MultiQuant 1.2 software (AB SCIEX) for automated LC-MS peak integration. All chromatographic peaks were manually reviewed for quality of integration and compared against a known standard for each metabolite to confirm compound identities. Internal standard peak areas were monitored for quality control, to assess system performance over time, and to identify any outlier samples requiring re-analysis. A pooled plasma reference sample was also analyzed after sets of 20 study samples as an additional quality control measure of analytical performance and to serve as reference for scaling raw LC-MS peak areas across sample batches. Metabolites with a signal-to-noise ratio <10 were considered below the limit of detection.

KCTD13 variant selection

To prioritize KCTD13 variants for functional analysis a differential density calculation was performed for each KCTD13 residue, which takes into account the density of population variants and the density of disease identified variants in a 10Å radius sphere around each amino acid in a protein's three-dimensional structure. Since no experimentally-solved structure exists for the complete KCTD13 protein, a homology model was built for human KCTD13 using the RaptorX webserver (http://raptorx.uchicago.edu)) (Kallberg et al., 2012). To build a complete homology model with existing structures, the KCTD13 sequence was divided into three domains (amino acids): domain 1(1 – 148), domain 2 (149 – 273), and domain 3 (274 – 329). Each domain was given a quality score by the RaptorX algorithm. P-value is the likelihood of a predicted model being worse than the best of a set of randomly-generated models for this protein (or domain), so P-value evaluates the relative quality of a model. The smaller the P-value, the higher quality the model. (For mainly alpha proteins, P-value less than 10^-3 is a good indicator. For manly beta proteins, P-value less than 10^-4 is a good indicator.) A crystal structure of domain 1 exists, pdb

4UIJ, Crystal structure of the BTB domain of KCTD13 (P-value= 1.1 x10^{-04}, Score = 110, uGDT/GDT= 113/76, uSeqID/SeqID= 104/70, ModelName= 4uijA-311804_1, Template= 4uijA) (Pinkas et al., 2017). Domain 2 was best fit to pdb 5e37, Redox protein from Chlamydomonas reinhardtii, (P-value 2.0 x10^{-03}, Score = 44, uGDT/GDT= 46/37, uSeqID/SeqID= 16/13, ModelName= 5e37A-311804_2, Template= 5e37A). Domain 3 was best fit to pdb 1FF4, X-ray structure of muscarinic toxin 2 at 1.5 Angstrom resolution, (P-value= 3.7e-02, Score= 6, uGDT/GDT= 13/24, uSeqID/SeqID= 6/11, ModelName= 1ff4A-311804_3, Template= 1ff4A) (Menez, R., Le Du, M.H., Gaucher, J.F., Menez, A. unpublished). Missense variants of KCTD13 from the genome aggregation database (gnomAD, v2.1.1) (population variants = 158 missense variants in 126 amino acid positions). Among these gnomAD variants are KCTD13 variants identified in schizophrenia individuals (Genovese et al., 2016), (disease-identified variants = 11 missense variants in 10 amino acid positions). These variants were mapped on the KCTD13 homology model using the framework underlying MISCAST (Iqbal et al., 2019). The density of disease-identified variants and density of population variants was computed within a 3D sphere (radius = 10Å) around each amino acid in the KCTD13 homology model. These densities were then normalized using the z-score function to identify the amino acid residues out of all residues that had a higher than average density of population and disease identified variants within this 3D proximity. We computed a normalized density difference score at each residue to detect hotspots, i.e. z-score(density of population variants around an amino acid) - z-score(density of pathogenic variants around an amino acid). Residues having a negative normalized densities difference were considered as “hotspot amino acids” (SUPP TABLE 4 and 5). In summary, the hotspots residues in 3D have an above-average density of disease-related variants than that of population variants within a spatial window (radius = 10Å).

Quantification and Statistical Analysis

Western blot quantification

Quantification of western blot signals for KCTD13, ADSS and ACTB was carried out in Image lab (Bio Rad) using the lane tools. Signals were normalized to ACTB and summary values were presented as mean +/- standard deviation.

Quantification of in-cell ubiquitination assays

Quantification of in-cell ubiquitin assay western blot images was carried out using the volume tools in the Image Lab software (Bio Rad). Equal rectangular regions were used to quantify each ADSS-myc-Ub signal in each lane. Input immunoblot KCTD13 signals were quantified using the lane tools of Image Lab and normalized to the ACTB signal. Each ADSS-myc-Ub signal was normalized to the KCTD13 western blot signal for each reaction. The reaction values were then normalized to the wild-type controls on the same blot. The results of three independent reactions were averaged to obtain the mean KCTD13 normalized ADSS-myc-Ub signal +/- standard deviation for wild-type and for each KCTD13 mutant.

Statistical analysis

Statistical details can be found in the Results, figure legends and figures for each experiment. For each experiment at least three biological replicates were performed. Unless otherwise indicated two-tailed Students tests were performed for each experiment and statistical significance was defined as $p<0.05$. Differential protein and K-ε-GG site abundances between *Kctd13*$^{-/-}$ and *Kctd13* WT neurons were identified using a moderated *t*-test using Bland-Altman filtering with the limma R-package (Ritchie et al., 2015) implemented in Protigy. *P* values were adjusted for multiple hypothesis testing using the Benjamini–Hochberg method. A two-way ANOVA was performed to test the interaction between L-alanosine and genotype on S-Ado levels.

Supplemental Materials References

Genovese, G., Fromer, M., Stahl, E.A., Ruderfer, D.M., Chambert, K., Landen, M., Moran, J.L., Purcell, S.M., Sklar, P., Sullivan, P.F.*, et al.* (2016). Increased burden of ultra-rare protein-altering variants among 4,877 individuals with schizophrenia. Nat Neurosci *19*, 1433-1441.

Iqbal, S., Jespersen, J.B., Perez-Palma, E., May, P., Hoksza, D., Heyne, H.O., Ahmed, S.S., Rifat, Z.T., Rahman, M.S., Lage, K.*, et al.* (2019). Insights into protein structural, physicochemical, and functional consequences of missense variants in 1,330 disease-associated human genes. bioRxiv 693259.

Kallberg, M., Wang, H., Wang, S., Peng, J., Wang, Z., Lu, H., and Xu, J. (2012). Template-based protein structure modeling using the RaptorX web server. Nat Protoc *7*, 1511-1522.

Pinkas, D.M., Sanvitale, C.E., Bufton, J.C., Sorrell, F.J., Solcan, N., Chalk, R., Doutch, J., and Bullock, A.N. (2017). Structural complexity in the KCTD family of Cullin3-dependent E3 ubiquitin ligases. Biochem J *474*, 3747-3761.

Ritchie, M.E., Phipson, B., Wu, D., Hu, Y., Law, C.W., Shi, W., and Smyth, G.K. (2015). limma powers differential expression analyses for RNA-sequencing and microarray studies. Nucleic Acids Res *43*, e47.